

RESEARCH

Open Access



Microglial heterogeneity in the ischemic stroke mouse brain of both sexes

Ángela del Águila¹, Ran Zhang¹, Xinyuan Yu¹, Lihong Dang¹, Feng Xu¹, Jin Zhang¹, Vaibhav Jain², Jilin Tian³, Xiao-Ping Zhong⁴, Huaxin Sheng¹ and Wei Yang^{1,5*} 

Abstract

Background Ischemic stroke elicits a complex and sustained immune response in the brain. Immunomodulatory treatments have long held promise for improving stroke outcomes, yet none have succeeded in the clinical setting. This lack of success is largely due to our incomplete understanding of how immune cells respond to stroke. The objective of the current study was to dissect the effect of permanent stroke on microglia, the resident immune cells within the brain parenchyma.

Methods A permanent middle cerebral artery occlusion (pMCAO) model was used to induce ischemic stroke in young male and female mice. Microglia were sorted from fluorescence reporter mice after pMCAO or sham surgery and then subjected to single-cell RNA sequencing analysis. Various methods, including flow cytometry, RNA in situ hybridization, immunohistochemistry, whole-brain imaging, and bone marrow transplantation, were also employed to dissect the microglial response to stroke. Stroke outcomes were evaluated by infarct size and behavioral tests.

Results First, we showed the morphologic and spatial changes in microglia after stroke. We then performed single-cell RNA sequencing analysis on microglia isolated from sham and stroke mice of both sexes. The data indicate no major sexual dimorphism in the microglial response to permanent stroke. Notably, we identified seven potential stroke-associated microglial clusters, including four major clusters characterized by a disease-associated microglia-like signature, a highly proliferative state, a macrophage-like profile, and an interferon (IFN) response signature, respectively. Importantly, we provided evidence that the macrophage-like cluster may represent the long-sought stroke-induced microglia subpopulation with increased CD45 expression. Lastly, given that the IFN-responsive subset constitutes the most prominent microglial population in the stroke brain, we used fludarabine to pharmacologically target STAT1 signaling and found that fludarabine treatment improved long-term stroke outcome.

Conclusions Our findings shed new light on microglia heterogeneity in stroke pathology and underscore the potential of targeting specific microglial populations for effective stroke therapies.

Keywords scRNA-seq, CD45 high, Stat1, Female, Microglia-to-macrophage

*Correspondence:

Wei Yang

wei.yang@duke.edu

Full list of author information is available at the end of the article



© The Author(s) 2024. **Open Access** This article is licensed under a Creative Commons Attribution-NonCommercial-NoDerivatives 4.0 International License, which permits any non-commercial use, sharing, distribution and reproduction in any medium or format, as long as you give appropriate credit to the original author(s) and the source, provide a link to the Creative Commons licence, and indicate if you modified the licensed material. You do not have permission under this licence to share adapted material derived from this article or parts of it. The images or other third party material in this article are included in the article's Creative Commons licence, unless indicated otherwise in a credit line to the material. If material is not included in the article's Creative Commons licence and your intended use is not permitted by statutory regulation or exceeds the permitted use, you will need to obtain permission directly from the copyright holder. To view a copy of this licence, visit <http://creativecommons.org/licenses/by-nc-nd/4.0/>.

Background

Ischemic stroke, a common and often devastating disease, remains poorly treated, highlighting the urgent need for new stroke therapies [1]. Clinical and experimental evidence points to neuroinflammation as a key element of stroke pathophysiology [2, 3]. Despite intense research in stroke immunology for decades, no immunomodulatory stroke therapeutic has been translated into clinical use [4]. This situation underlines key gaps in our understanding of the stroke-induced immune response.

Microglia, the resident immune cells in the brain parenchyma, play a key role in mediating and orchestrating neuroinflammation following stroke [5, 6]. Surprisingly, the precise role of activated microglia in stroke is still debated, with evidence supporting both detrimental and beneficial effects. For example, many stroke treatment experiments have attributed the observed protective effects to the suppression of microglia activation [7]. It is thought that after stroke, activated microglia secrete inflammatory cytokines and chemokines, exacerbating the immune response in the brain and promoting neuronal death. On the other hand, studies have shown that pharmacologic depletion of microglia results in elevated inflammatory response, larger infarcts, and worse functional outcome after stroke, suggesting a potential beneficial role of microglia in the acute stroke phase [8]. Collectively, the impact of microglia on stroke progression remains elusive. This complexity arises from the dynamic and diverse states that microglia can adopt in response to stresses [9]. It is reasonable to assume that different microglial states may play distinct roles in stroke pathology. Therefore, conflicting results regarding microglia in stroke are likely due to indiscriminate targeting of mixed microglial subsets.

To address these complexities, the stroke field has embraced single-cell RNA sequencing (scRNA-seq) to categorize distinct immune cell subsets in the stroke brain based on transcriptional profiles. Indeed, these scRNA-seq studies have revealed highly heterogeneous immune cell populations, including various states of microglia in the stroke brain [10–17]. However, these studies used either all brain cells or enriched CD45⁺ immune cells, which likely limits the depth of identifying microglial subsets. More critically, in the stroke brain, certain microglia subpopulations and infiltrating monocytes share similar phenotypes, which confounds accurate annotation of these cells. In our current study, we took advantage of a mouse genetic tool, *Tmem119-2A-CreERT2*, which expresses Cre highly specific to microglia in the brain [18]. Fluorescence-labeled microglia in the stroke brain were sorted and then subjected to scRNA-seq analysis. Of note, previous

scRNA-seq studies exclusively used transient ischemic stroke models, which do not represent the majority of clinical stroke cases [19]. In light of this, we opted to use our permanent ischemic stroke model [13, 20]. Moreover, as sex differences in stroke outcome are well supported by clinical and experimental findings, and as animal studies also suggest sexual dimorphism in the neuroinflammatory response after stroke [21, 22], we included both male and female animals. Our data demonstrate that microglia responded to permanent stroke similarly in male and female mice. Importantly, our findings revealed several stroke-associated microglial (SAM) subsets that could serve as a foundational framework for further studies aimed to understand microglial functions in stroke. Of these subsets, one unique subset may represent the long-sought stroke-induced CD45 high microglia subpopulation. Lastly, our functional outcome study suggests that the interferon (IFN) signaling-associated microglia subset is detrimental to stroke recovery.

Methods

Animals

All animal procedures were approved by the Duke University Medical Center Animal Care and Use Committee and were conducted in accordance with the United States Public Health Service's Policy on Humane Care and Use of Laboratory Animals. The animals were maintained in a 14/10 light/dark cycle, and both water and food were provided ad libitum. Male and female C57Bl/6 mice (3–6 months old) were purchased from The Jackson Laboratory (Bar Harbor, ME). To establish mice with inducible labeling of microglia in the brain, we crossbred Ai6 (RCL-ZsGreen; JAX #007906) reporter mice with *Tmem119-2A-CreERT2* mice (JAX #031820) expressing the tamoxifen-inducible CreERT2 under control of the *Tmem119* promoter and obtained *Tmem119-2A-CreERT2;Ai6* (*Tmem119-Ai6*) mice. To fluorescently label immune cells, we generated *Vav1-Cre;Ai9* mice by crossing *vav-Cre* (JAX #035670) with *Ai9* (RCL-tdTomato; JAX #007909). Mice were euthanized via decapitation while fully anesthetized. All mouse lines were on a C57Bl/6 genetic background.

Stroke surgery

Permanent middle cerebral artery occlusion (pMCAO) was performed according to our previously established procedure [20, 23]. In brief, mice were anesthetized with 5% isoflurane in a mixture of 30% O₂/70% N₂, followed by oral intubation. Ventilation (Kent Scientific) was adjusted based on the body weight with 1.2–1.5% isoflurane throughout the surgery. The body temperature was monitored with a rectal probe and maintained at 37 °C ± 0.2 °C

for the entire duration of the surgery. Mice were placed in a left lateral position, and a small transverse incision was made between the eye and ear to reveal the zygomatic arch. A segment of approximately 3 mm from the zygomatic arch was excised, and a small opening was drilled on the skull to expose the MCA. The MCA trunk was then permanently ligated with a silk suture. Following MCAO, the animals were kept under anesthesia for 1 h and then transferred to a chamber (32 °C) and monitored for a 2-h recovery period before returning them to their home cages. No animal was excluded for analyses in this study.

Stroke outcome

Animals were randomized into groups using an online tool, and stroke outcome, including neurologic functions and infarct volume, was assessed at indicated time points after pMCAO by experimenters who were blind to groups.

Neurologic score [24]

A 48-point neurologic scoring system was used to evaluate various functions including general status (spontaneous activity, body symmetry, and gait; 0–12), simple motor deficit (forelimb asymmetry, circling, and hind-limb placement; 0–14), complex motor deficit (vertical screen climbing, and beam walking; 0–8), and sensory deficit (hind limb, trunk, vibrissae, and face touch; 0–14).

Rotarod [25]

Mice were trained for 3 days before surgery, to establish similar baseline performance. On the test day, mice were placed on an accelerating rod (4–40 rpm; Ugo Basile, Italy). The latency time to fall off the rod was recorded.

Pole test [25]

Mice were placed on top of a vertical pole (50 cm high) with their heads oriented upward. The time required for mice to arrive at the base of the pole (time-to-arrive) was recorded.

Y maze

A spontaneous alternation Y maze test was used to examine spatial memory. The Y maze apparatus (San Diego Instruments, Beige 7001–0425) consists of 3 identical arms (15-inch length, 3-inch width, 5-inch height) with 120° angles. Three different visual cues were attached to the end wall of each arm. Mouse was placed in the center and allowed to explore freely for 5 min, while it was video recorded. The spontaneous alternation score was calculated using the equation: sequential alternations/total arm entries - 1.

Infarct measurement [20]

After behavioral tests were completed, mice were euthanized, and infarct volume was measured using the 2,3,5-triphenyltetrazolium chloride (TTC; Sigma-Aldrich, St. Louis, MO, USA) staining method. Infarct volume was calculated using ImageJ software (NIH).

Drug administration

To induce CreER-dependent recombination, Tmem119-Ai6 mice received tamoxifen (20 mg/kg) intraperitoneally (ip) once daily for 5 days. After a minimum waiting period of 1 week, the mice were then used for experiments. To label newly proliferative cells *in vivo*, animals were injected ip with BrdU (Sigma, #59,143; 100 mg/kg) starting immediately after the stroke surgery and continuing for two additional days. For the fludarabine (S1491, Selleck Chemicals) treatment experiments, the vehicle (5% DMSO, 40% PEG300, 5% Tween 80, and 50% saline) and dosage (5 mg/kg for the short-term experiment and 10 mg/kg for the long-term experiment) were based on a previous study, with minor modifications [26].

Flow cytometry

Profiling immune cells in the brain and blood was performed by flow cytometry, following our standard protocols with modifications [13, 27].

To prepare single-cell suspensions from the brain, the mice were transcardially perfused with ice-cold PBS, and the brains were rapidly isolated. For the stroke mice, the brains were split into ipsilateral and contralateral hemispheres along the midline. The brains were then mechanically homogenized in ice-cold HBSS using a loose pestle in a 15-mL Dounce homogenizer (Kimble). The resultant cell suspension was filtered through a pre-wet 70- μ m cell strainer. After centrifugation, cells were resuspended in 8 mL of ice-cold 35% Percoll (Cytiva, #17-089-101) in PBS and centrifuged at 845 \times g for 20 min at 4 °C with the speed of acceleration and braking set at 3 out of 9 levels. The cell pellet was washed and resuspended in FACS buffer (RPMI1640, 2% FBS, and 2 mM EDTA). For blood samples, red blood cells were lysed with 1X RBC lysis buffer (BioLegend) and cells were resuspended in PBS buffer with 2% FBS.

For flow cytometry, single-cell samples were incubated with Fc Block TrueStain (BioLegend, #101320) at 4 °C in the dark for 15 min. Then, an antibody mixture was added for immunostaining with incubation for 30 min at 4 °C. Next, cells were pelleted and resuspended in HBSS buffer with a live/dead fixable dye for 10 min. After washing, cells were resuspended in FACS buffer for analysis. For phagocytosis assay, cells were incubated with antibodies and Zymosan bioparticles (ThermoFisher,

P35364) for 1 h at 37 °C. After centrifugation, cells were resuspended in FACS buffer and 5 min prior to data acquisition 7-AAD was added to evaluate cell viability. Flow cytometry data were acquired on FACS Canto (BD Biosciences, San Jose, CA) or Aurora full spectrum flow cytometer (Cytek Biosciences, Fremont, CA) and analyzed using SpectroFlo and FlowJo software. All antibodies are listed in Additional file 1: Table S1.

Bone marrow transplantation (BMT)

Mice were anesthetized using ketamine/xylazine and irradiated with a single dose of sublethal irradiation (950 cGy) with the brain shielded in a cabinet X-ray irradiator (CIX3, Xstrahl, Suwanee, GA, USA). Five hours after irradiation, mice received a retro-orbital injection containing 5×10^6 bone marrow (BM) cells from a donor mouse of matching sex and age. We adopted a simple protocol to prepare BM cells [28]. Briefly, mouse limbs were collected and placed in ice-cold PBS. After removing the muscles, the bones were put in a 500- μ L tube with a hole punched in the bottom. This tube was inserted into a 1.5-mL tube containing 100 μ L of PBS. After centrifugation (10,000 \times g, 30 s, 4 °C), BM cells were collected in the 1.5-mL tube and subjected to red blood cell lysis using RBC lysis buffer (BioLegend). The BM cells were washed, resuspended in PBS, and counted. For BMT, recipient mice were anesthetized using a mixture of 1.5–2.0% isoflurane in 30% O₂/70% N₂, and the cells from the donor were administered via retro-orbital injection.

Immunofluorescence and microscopy

Mice were transcardially perfused with ice-cold PBS followed by 4% PFA. The brains were then harvested, immersed in 4% PFA overnight, and transferred to PBS for vibratome sectioning. Immunostaining was performed as described previously [20]. Briefly, after blocking, coronal brain sections (50 μ m thick) were incubated with primary antibodies (Additional file 1: Table S1) overnight at 4 °C. The next day, samples were washed in PBS with 0.1% Triton (5 min \times 3) and then incubated with fluorescent secondary antibodies for 2 h at room temperature (RT). Nuclear staining with 4',6-diamidino-2-phenylindole (DAPI) was then performed for 10 min at RT. For BrdU staining, an additional step for sample preparation was required: the brain sections were incubated with freshly made 2 N hydrochloric acid (HCl) for 30 min and washed thoroughly with PBS. Images were captured on a Zeiss Axio Imager Z2 motorized fluorescence microscope (Carl Zeiss MicroImaging) or a Leica SP5 confocal microscope.

Hybridization chain reaction (HCR) RNA fluorescence in situ hybridization (FISH)

After perfusion with PBS and 4% PFA, the mouse brains were incubated with 4% PFA overnight and then transferred to DEPC-treated PBS for vibratome sectioning. Coronal brain sections (50 μ m) were washed with 4% PFA and stored in DEPC-treated PBS at 4 °C until analysis. For HCR RNA-FISH, all probes and reagents were purchased from Molecular Instruments. On day 1, the brain sections were incubated in 500 μ L of 70% ethanol in DEPC-treated PBS at 4 °C in a 24-well plate overnight. The next day, the sections were washed with PBS and then incubated in 5% SDS for 45 min at RT on an orbital shaker. The brain sections were then washed with 2xSSC buffer and incubated in the same solution for 15 min at RT on the orbital shake. Next, the sections were incubated in hybridization buffer for 30 min at 37 °C, followed by 24-h incubation at 37 °C with a pre-warmed mixture of the designed probes (*Spp1*, *Arg1*, *Mki67*, or *Isg15*; a final concentration of 5 mM) in probe hybridization buffer. On the third day, the sections were first washed (37 °C, 15 min \times four times) using probe wash buffer pre-warmed at 37 °C, then washed with 2xSSC (5 min, RT, on the orbital shaker), and incubated with HCR amplification buffer for 30 min (RT, on the orbital shaker). To perform HCR, fluorescent hairpins were heated at 95 °C for 90 s in a thermocycler, followed by cooling at RT for 30 min in the dark. Then, 4 μ L of hairpin H1 and 4 μ L of hairpin H2 (B1-647, B2-594 systems) per 300 μ L were mixed and added to the samples. The floating sections were then incubated at 26 °C for 24 h. On the fourth day, the sections were washed with 2xSSC and stained with DAPI. Finally, the brain sections were mounted on slides using Fluoromount-G mounting medium (Southern Biotech, 0100–01). Images were acquired using a Leica SP5 Inverted Confocal Microscope or a Zeiss Axio Imager microscope.

3D whole-brain imaging

Whole-brain clearing, immunolabeling, and imaging were performed by LifeCanvas (Cambridge, MA) following established protocols. Briefly, PFA-fixed brains were preserved using SHIELD reagents [29]. After delipidation, samples were labeled using eFLASH technology in a SmartLabel device (LifeCanvas). After immunolabeling, samples were incubated in 50% EasyIndex (RI = 1.52, LifeCanvas) overnight at 37 °C followed by 1-day incubation in 100% EasyIndex for refractive index matching. The brain samples were imaged using a SmartSPIM axially swept light sheet microscope with a 3.6 \times (0.2 NA). Samples were registered to the Allen Brain Atlas using an automated process (alignment performed by LifeCanvas

Technologies). A NeuN channel for each brain was registered to an average NeuN atlas (generated by LifeCanvas Technologies using previously registered samples). Registration was performed using successive rigid, affine, and b-spline warping algorithms (SimpleElastix: <https://simpleelastix.github.io/>). Imaris v9.0 was used for 3D rendering and creating videos.

Single-cell RNA sequencing (scRNA-seq) analysis

The scRNA-seq analysis was completed at Duke Molecular Genomics Core (MGC) following established protocols. The overall workflow for sample preparation, RNA sequencing, and data analysis was largely similar to our previous study [13].

Briefly, each hemisphere was mechanically homogenized with a Douncer. To enrich immune cells and remove myelin, the cells were resuspended in 37% Percoll (Cytiva) layered on 70% Percoll in PBS in a 15-mL tube. After centrifugation, the supernatant containing myelin and debris was removed and the interphase between the 37% and 70% Percoll layer was collected and washed. Eventually, the cells were resuspended in 500 μ L of FACS buffer. Of note, the 500- μ L cell suspension included a pool of four mice per condition. Next, 1 μ L of 7-AAD was added per sample to stain dead cells. Live *ZsGreen*⁺ cells were sorted on a BD FACSAria II with a purity mode. FACS-isolated cells were immediately delivered to Duke MGC for library preparation.

The protocols for library preparation and RNA sequencing were essentially the same as described previously [13]. Briefly, a 10 \times Genomics Chromium Controller Single-Cell Instrument (10 \times Genomics, Pleasanton, CA, USA) was used to generate single-cell gel beads with reverse transcription (RT) reagents in emulsions (GEMs). After GEM-RT was performed, the single-strand cDNA was purified with DynaBeads MyOne Silane Beads (Thermo Fisher Scientific). The cDNA was then amplified and purified. Indexed sequencing libraries were constructed using the Chromium Single-Cell 3' v3.1 Library Kit following the manufacture's instruction. The bar-coded sequencing libraries were quantified and loaded on a Novaseq 6000 (Illumina, San Diego, CA, USA) for sequencing. The dataset has been deposited in NCBI Gene Expression Omnibus (GEO) database repository with the accession number GSE267240 [30].

Bioinformatics processing and data analysis

Bioinformatics processing and data analysis were performed as described previously with modifications [13]. Briefly, Cell Ranger software version 6.1.2 was used for initial data processing. A custom reference transcriptome was created by adding the *ZsGreen* gene sequence

to mouse mm10-2020-A transcriptome using `cellranger mkref()` function. The secondary statistical analysis was performed using an R package Seurat version 4.9 which performed quality control and subsequent analyses on the feature-barcode matrices produced by Cell Ranger. In Seurat, cells not expressing *ZsGreen* were filtered out (*ZsGreen* $\text{exp} < 0$). We then closely examined the data and performed further filtering based on a range of metrics (% mitochondrial expression < 30 , $250 < n\text{Feature} > 8000$, $500 < n\text{UMI}(\text{count}) > 50,000$ for all samples) to identify and exclude possible multiplets (i.e., instances where more than one cell was present and sequenced in a single emulsified gel bead). To further remove doublets/multiplets, DoubletFinder (version 2.0.3) was used in R individually on each sample [31]. The removal of further technical artifacts was performed using regression methods to reduce noise. Downstream analysis for linear dimensional reduction, integration, clustering, visualization, and comparison between samples was performed as described previously [13]. For the module score analysis, `AddModuleScore` function in the Seurat package was used to compute the functional signatures for each cell cluster. Module scores were based on the gene lists shown in Additional file 1: Table S2. Visualization of the module scores used the `ggplot2` package (v3.4.3) in R. To generate the heatmap, the top 10 upregulated genes for clusters 7–13 were identified using the `FindAllClusters` function in the Seurat package, applied to a comprehensive dataset of 15 clusters. The dataset was then filtered to retain only clusters 7–13, and the `FindAllClusters` function was reapplied to identify the top 10 genes with the highest average log-fold changes within these specific clusters. The data were visualized using the `ComplexHeatmap` package (v2.10.0) in R. We employed the `CellChat` (v2.0.0) package to explore and visualize the cell–cell communication network, focusing on the CCL pathway across clusters 1–13. To examine the intercellular communication relationship between clusters (1–13), cell–cell interaction networks were constructed with the custom mouse ligand-receptor databases in CellChat. The gene expression matrix for clusters 1–13 was extracted from the processed Seurat object for this analysis. Then, it was processed using the standard pipeline. The communication probabilities of ligand-receptor interactions were calculated using the `computeCommunProb` function with “truncatedMean” as the method to compute the average gene expression. We then filtered out interactions with less than ten cells in each cluster using the `filterCommunication` function. The `netVisual_chord_cell` function was used to visualize the CCL signaling network for clusters 1–13. The result was visualized through a chord diagram using the CellChat package in R.

Statistical analysis

All statistical analyses were performed using GraphPad Prism 9. Infarct volume (short-term) or neurologic score (long-term) was used to determine the group size for stroke outcome experiments. Statistical differences between groups were evaluated by unpaired Student's *t*-test, Mann–Whitney *U* test (neurologic scores), or an ANOVA one-way followed by Holm–Sidak post hoc test. Data were presented as median or mean \pm SD. *P*-values < 0.05 were considered significant.

Results

Morphologic and spatial changes in microglia in the stroke brain revealed by Tmem119-Ai6 mice

To study the microglial dynamics in the stroke brain, we first performed Iba1 staining of the brains collected on post-stroke days 1, 3, and 7 (Additional file 1: Fig. S1). We also compared males and females on day 3 after stroke. Iba1⁺ cells started to accumulate in the peri-infarct regions on day 3 after permanent stroke, and on day 7, a large number of Iba1⁺ cells were present in the infarct core (Additional file 1: Fig. S1A), consistent with previous studies [32, 33]. Quantitative analysis revealed that in the infarct core, there were few Iba1⁺ cells on day 1, but their numbers markedly increased on day 7 after stroke (Additional file 1: Fig. S1B,C). Moreover, our analysis indicated that there was no difference in Iba1⁺ cell numbers between males and females across the regions on day 3 after stroke. We also did not observe obvious morphologic differences in Iba1⁺ cells between sexes (Additional file 1: Fig. S1D), aligning with previous data [34]. Since microglia share many cell surface markers and molecular profiles with infiltrating monocytes/macrophages, it is expected that not all Iba1⁺ cells in the stroke brain are microglia. Therefore, we decided to use a microglia-specific reporter mouse line to study the role of microglia in stroke. Recently, Tmem119 has been identified as a homeostatic microglial marker in the brain, and thus, we chose to use Tmem119-CreERT2 mice to dissect the effects of stroke specifically on microglia in this study [18]. Of note, this mouse Cre-driver line is tamoxifen-inducible, which allowed us to label the microglia already present in adult mice before stroke.

We first crossbred Tmem119-CreERT2 mice with ZsGreen reporter Ai6 mice to generate Tmem119-Ai6 (Fig. 1A). To specifically label microglia with ZsGreen, Tmem119-Ai6 were treated with tamoxifen. Consistent with previous reports, the ZsGreen signal was ubiquitously evident across the whole brain, and ZsGreen⁺ cells exhibited typical microglial morphology and were co-localized with Iba1 (Fig. 1A and Additional file 1: Fig. S2A). In the healthy brain, microglia are believed to reside in the CD45^{Lo}CD11b⁺ gate of flow cytometry analysis.

Indeed, in the Tmem119-Ai6 mouse brain, approximately 96.7% of CD45^{Lo}CD11b⁺ cells expressed ZsGreen, and 99.7% of ZsGreen⁺ cells are CD45^{Lo}CD11b⁺, confirming that microglia are specifically and almost completely labeled with ZsGreen in the Tmem119-Ai6 mouse brain (Fig. 1B). We then performed more detailed immunophenotyping of ZsGreen⁺ cells in the circulation. In the blood, we detected a negligible population (0.69%) of CD45⁺ cells expressing ZsGreen, mainly consisting of monocytes (Fig. 1C and Additional file 1: Fig. S2B).

Compared to traditional Iba1 staining, Tmem119-Ai6 mice enable us to clarify morphologic and spatial changes specifically in microglia after stroke. Thus, we used Tmem119-Ai6 mice to examine microglia on days 1, 3, and 7 after permanent stroke. Notably, the dynamic changes in microglia are similar to those observed in our Iba1 staining (Additional file 1: Fig. S1). On day 1 after stroke, we observed a noticeable decrease in the ZsGreen signal in the infarct core, along with a slight increase in the number of ZsGreen⁺ cells in the peri-infarct area. On post-stroke day 3, many ZsGreen⁺ cells accumulated bordering the infarct, while on day 7, these cells appeared to have migrated into the infarct core, displaying an intensified fluorescence signal (Fig. 1D). Immunostaining analysis further confirmed microglial specificity of the ZsGreen signal in the stroke brain (Fig. 1E and Additional file 1: Fig. S2C). As expected, the morphology of many microglia in the ipsilateral hemisphere changed from a ramified structure to an amoeboid one (Additional file 1: Fig. S2D).

Next, to gain a better visualization of the spatial pattern of microglia in the stroke brain, we imaged cleared whole brains, especially on day 3 after stroke. Moreover, to examine infiltrating immune cells concurrently, we performed bone marrow transplantation (BMT) from Vav1-Ai9 donor mice into Tmem119-Ai6 mice (Fig. 2A). Of note, in Vav1-Ai9 mice, most peripheral immune cells were labeled with tdTomato. After BMT, we confirmed that ~70% of CD45⁺ cells in the blood of BMT chimera mice were tdTomato⁺ (Additional file 1: Fig. S3). The brains of these chimera mice were collected on days 1 and 3 after permanent stroke, cleared, and stained with NeuN for whole-brain imaging (Fig. 2). Consistent with the findings in Fig. 1, there were only subtle changes in the overall pattern of microglia in the non-infarct area on day 1 after stroke (Fig. 2B; Additional file 2: Movie S1). However, on day 3, the number of microglia surrounding the infarct core markedly increased (Fig. 2B; Additional file 3: Movie S2; Additional file 4: Movie S3). Similarly, on day 1, only a small amount of infiltrating immune cells (tdTomato⁺) was found in the stroke brain. In contrast, we observed a large quantity of tdTomato⁺ cells in the stroke brain on day 3 (Fig. 2C; Additional file 3:

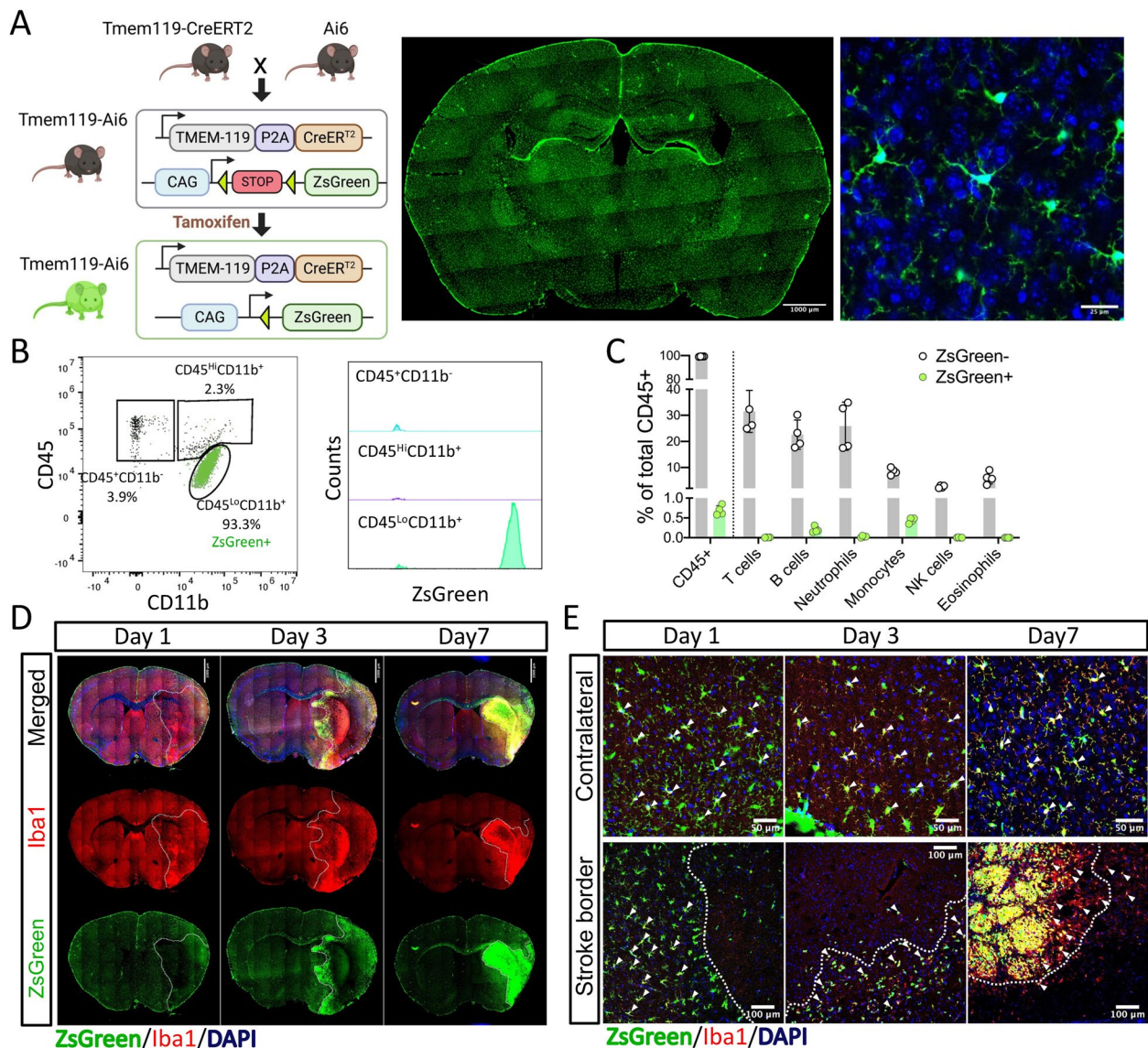


Fig. 1 Microglia in the stroke brain revealed by Tmem119-Ai6. **A** Schematic overview of Tmem119-Ai6 mice. After tamoxifen treatment, ZsGreen is specifically expressed in the microglia in the brain of Tmem119-Ai6 mice. A representative native fluorescence image of a coronal section of a Tmem119-Ai6 brain shows the widespread ZsGreen signal (green) throughout the brain, and a confocal image depicts the typical microglia morphology of ZsGreen⁺ cells (DAPI: blue). **B, C** Flow cytometry analysis of ZsGreen⁺ cells in the brain and blood. In the Tmem119-Ai6 brain, almost all CD45^{lo}CD11b⁺ cells are ZsGreen positive (**B**). In the blood, only a negligible population of CD45⁺ cells, primarily monocytes, are ZsGreen positive (**C**). Data are presented as mean ± SD (*n* = 4/group). **D, E** Dynamic changes in microglia in the brain of Tmem119-Ai6 mice after ischemic stroke. Tmem119-Ai6 mice were subjected to permanent stroke. The brains were collected on days 1, 3, and 7 after stroke for immunostaining. **D** Overview of coronal brain sections of Tmem119-Ai6 mice after stroke. In addition to native ZsGreen fluorescence (green), the brain sections were also stained with Iba1 (red) and DAPI (blue). **E** Confocal images showing colocalization of Iba1 and ZsGreen signals. Images are representative from two mice per time point. Dot lines depict the stroke border

Movie S2). Our flow cytometry analysis confirmed this increase (Additional file 1: Fig. S4). Interestingly, unlike microglia (ZsGreen⁺), these tdTomato⁺ cells spread relatively evenly across the stroke area including the infarct core and peri-infarct regions (Fig. 2C). Considering

the strong ZsGreen signal in the infarct core on day 7 (Fig. 1D), it is likely that in the subacute phase (post-stroke day 7), microglia are the primary cells that clear cell debris in the infarct. Indeed, the phagocytic capacity of microglia was markedly increased on day 7 after stroke

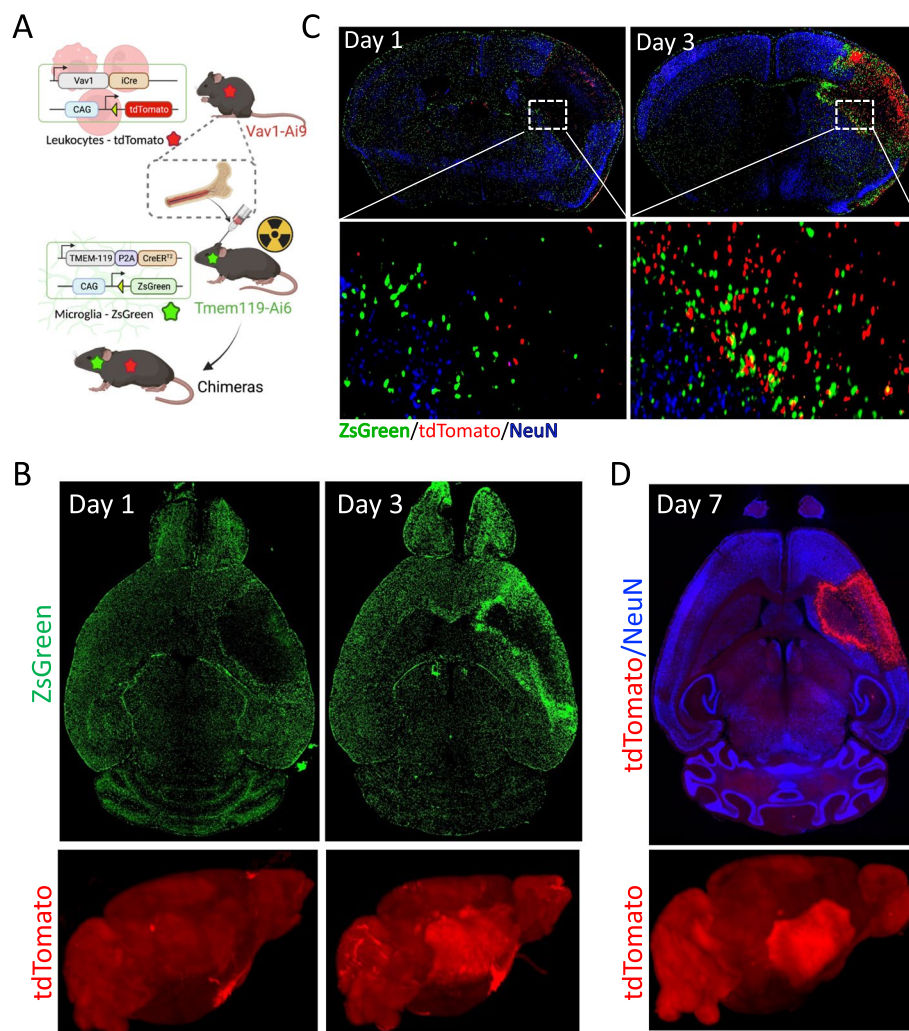


Fig. 2 Whole-brain imaging of microglia and infiltrating immune cells after ischemic stroke. **A** Schematic representation of bone marrow transplantation. The bone marrow from Vav1-Ai9 mice was transplanted into Tmem119-Ai6 mice to obtain chimeric mice with microglia labeled with ZsGreen (green), and periphery immune cells labeled with tdTomato (red). **B** Microglia and infiltrating immune cells in the stroke brain. Chimeric mice were subjected to permanent stroke. On days 1 and 3 after stroke, the brains were collected for whole brain imaging. Transverse views of microglia (ZsGreen; above) and 3D whole-brain views of infiltrating immune cells (tdTomato; below) are shown here. **C** Microglia and infiltrating immune cells in the peri-infarct area. Enlarged images are shown below. **D** A chimeric mouse with periphery immune cells labeled with tdTomato (red) was subjected to permanent stroke. The brain was collected on post-stroke day 7. Associated videos are available in the supplemental materials

(Additional file 1: Fig. S5). To further support this, we imaged the whole brain of a chimera mouse with BMT from Vav1-Ai9 into wild-type mice on day 7 after stroke. Indeed, in this subacute phase, most infiltrated immune cells (tdTomato⁺) were found in the peri-infarct area (Fig. 2D; Additional file 5: Movie S4). A side-by-side comparison of infiltrating immune cells at these three time points is shown in Additional file 1: Fig. S6. Together, our data provided a comprehensive and definitive picture of the dynamic changes of microglia, as well as infiltrating immune cells, in the brain after permanent stroke.

Initial assessment of scRNA-seq data on microglia from male and female mouse brains after permanent stroke

We then asked two questions: how does permanent stroke impact the cellular heterogeneity of microglia, and do microglia respond to stroke differently in male vs female? To address these questions, we leveraged scRNA-seq analysis (Fig. 3). On day 3 after permanent MCAO or sham, we enriched ZsGreen⁺ cells from male and female Tmem119-Ai6 mouse brains by FACS. To minimize transcriptional changes during cell preparation, all steps

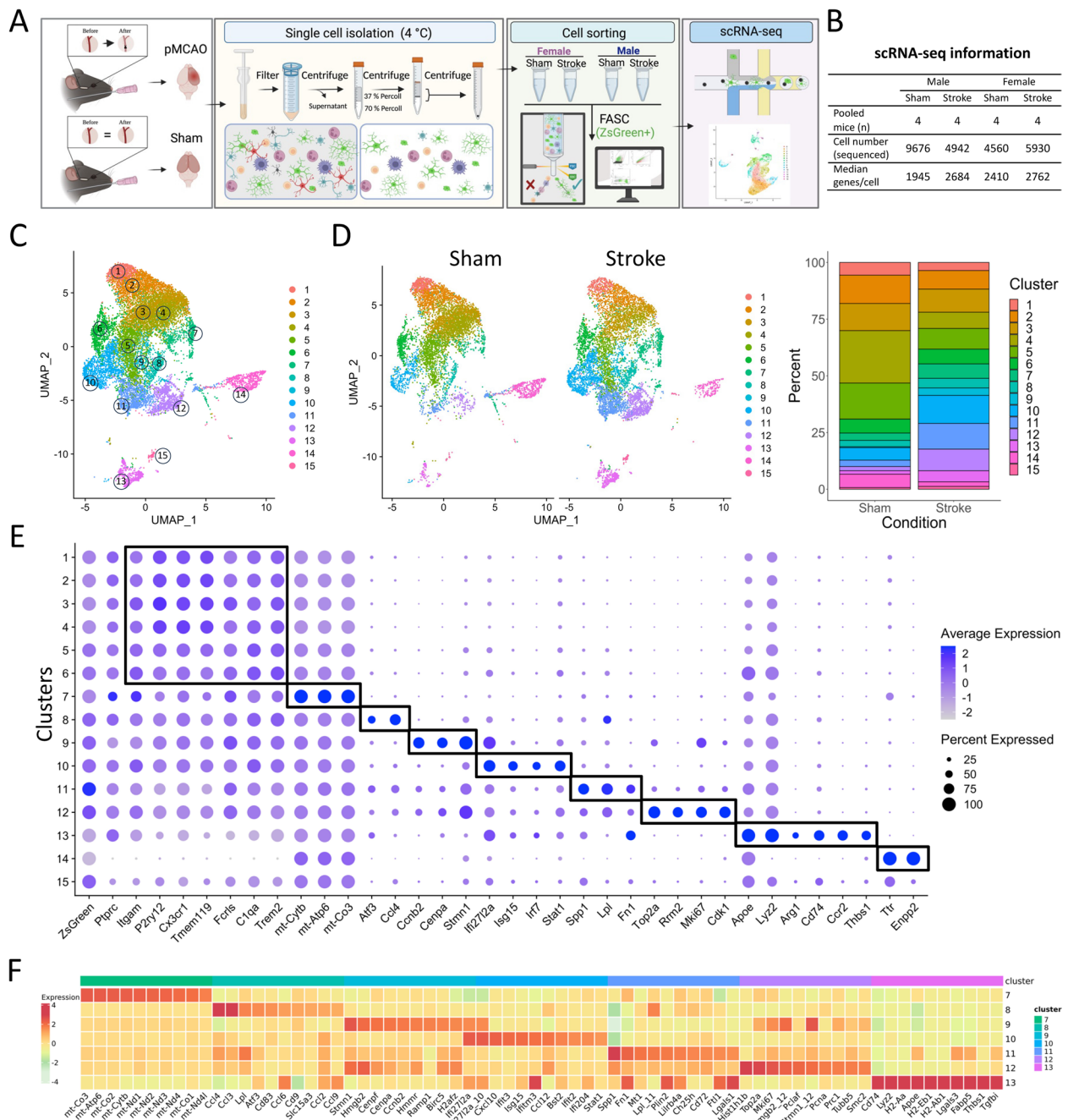


Fig. 3 Single-cell RNA sequencing (scRNA-seq) analysis of microglia in the stroke brains of male and female mice. **A** Scheme of the experimental design for scRNA-seq analysis. Male and female mice ($n=4$ /group) were subjected to permanent stroke or sham. Three days later, ipsilateral (stroke) or both (sham) hemispheres were collected for cell sorting and scRNA-seq analysis. **B** Data table summarizing scRNA-seq analysis. **C** UMAP plot of aggregated data from all groups. **D** Split view of UMAP plots of sham and stroke groups. Stacked bar plots (right) depict the proportions of microglia subsets in sham and stroke brains. **E** Dot plot showing the scaled expression of selected genes for each cluster. Cluster numbers were assigned manually. Dot size indicates proportion of cells within the cluster, and color intensity reflects average expression levels. **F** Heatmap showing the top 10 upregulated genes in stroke-related microglial clusters 7–13

were performed on ice or at 4 °C. To account for surgical and biological variations, the cells for each sample were pooled from four mice. The basic information of this scRNA-seq experiment is shown in Fig. 3B.

For data analysis, we first excluded ZsGreen-negative cells to ensure downstream analysis of microglia only. Unsupervised clustering on the aggregate sequencing data identified 20 transcriptionally distinct clusters.

We then removed 5 clusters due to the small cell numbers (<50 cells). The remaining 15 clusters are shown in the uniform manifold approximation and projection (UMAP) plot (Fig. 3C), and their top 50 differentially expressed gene (DEG) cluster markers are listed in Additional file 6: Table S3. The split UMAP plots and stacked bar plots illustrated proportion changes in each colored cluster after stroke (Fig. 3D). Selected marker genes for each cluster are shown in Fig. 3E, except cluster 15 that could not be defined due to lack of prominent molecular markers. Further, cluster 14 cells did not express any microglial genes, but showed high expression of some epithelial cell genes (e.g., *Ttr* and *Enpp2*) [35], likely originating from the choroid plexus. Thus, only clusters 1–13 were discussed in the following analyses. Since microglial polarization with M1 or M2 phenotype is a frequently used paradigm in studying stroke-induced microglial activation, we inspected a few commonly used M1/M2 markers in our dataset and did not find any cluster that can clearly be annotated as M1 or M2 microglia (Additional file 1: Fig. S7A). In fact, these genes were largely absent in most microglia, except for cluster 13 (a macrophage-like cluster; see below). Next, we performed an analysis of DEGs and processes/pathways associated with stroke (Additional file 1: Fig. S7B,C). A total of 174 genes (127 upregulated; 47 downregulated) showed ≥ 1.5 -fold change (stroke vs sham; $p_{\text{adj}} < 0.01$) (Additional file 1: Fig. S7B; Additional file 7: Table S4). The upregulated genes (e.g., *Spp1*, *Lpl*, and *Stmn1*) and processes/pathways (e.g., translation and response to interferon) reflected an increase in the frequency of clusters in the stroke brain. As expected, the downregulated genes included microglial homeostatic genes (e.g., *Tmem119*, *P2ry12*, and *Cx3cr1*), as microglial genes are reportedly downregulated after activation [36]. The significantly enriched pathways were related to cell migration, phagocytosis, and interferon response (Additional file 1: Fig. S7C; Additional file 7: Table S4). Lastly, based on the percentage change of each cluster (Additional file 1: Fig. S8A), we considered clusters 1–6 as homeostatic microglia (representing 75.2% in sham and 44.7% in stroke samples), while clusters 7–13 represented stroke-related microglial states (24.8% in sham and 55.3% in stroke samples). This classification was also supported by a decrease in the expression of canonical microglial genes (e.g., *Tmem119*, *P2ry12*, and *Cx3cr1*) in clusters 7–13 (Additional file 1: Fig. S8B). The top 10 upregulated genes for clusters 7–13 are shown in Fig. 3F. Since clusters 10–12 appeared to be the major microglial clusters induced by stroke and cluster 13 displayed a unique gene profile (see below), we decided to focus on clusters 10–13 in the current study.

However, it is noteworthy that many mitochondria genes were upregulated in cluster 7 (Fig. 3F and Additional file 1: Fig. S8C), and cluster 8 is likely a major microglial population producing chemokines and modulating other immune cells in the stroke brain (Fig. 3F and Additional file 1: Fig. S8D,E).

No major difference in microglial response to stroke in male vs female mice

Next, we set out to assess the potential sex differences in microglial response to stroke. To establish the effect of sex in our permanent stroke model, we first performed a stroke outcome study using male and female mice (Additional file 1: Fig. S9). Female mice exhibited significantly better neurologic scores than male mice on day 3 after pMCAO (Additional file 1: Fig. S9A). However, in the rotarod test, male and female mice behaved similarly (Additional file 1: Fig. S9B). Critically, we did not see a significant difference in infarct size between the two groups (Additional file 1: Fig. S9C), consistent with a previous study [37]. Overall, male and female mice had similar brain damage after permanent stroke.

We then analyzed the scRNA-seq data from individual groups. As expected, *Xist* and *Tsix*, two long non-coding RNAs involved in X chromosome inactivation, were present only in microglia from females, while male microglia expressed the Y chromosome genes *Eif2s3y* and *Ddx3y* (Additional file 1: Fig. S10A). As shown in the UMAP plots, all clusters were present in both male and female groups and exhibited similar patterns (Fig. 4A). Stroke-induced changes in the percentage of each cluster were comparable between sexes as well (Fig. 4B and Additional file 1: Fig. S10B). This comparability also attested the reproducibility of our scRNA-seq analysis. Further, most of the DEGs (stroke vs sham) were shared in males and females (Fig. 4C,D). Specifically, with a threshold of 1.5-fold increase (stroke vs sham), a total of 148 and 126 DEGs were identified for females and males, respectively, with 102 in common between sexes (Additional file 8: Table S5). Consistently, the comparison of male vs female in stroke groups only identified sex-specific genes (Additional file 1: Fig. S10C). However, we did note that many mitochondrial genes involved in the respiratory chain (e.g., *mt-Nd3*, *mt-Cytb*, *mt-Co1-3*, and *mt-Atp6*) were upregulated in female vs male microglia of the sham groups (Additional file 1: Fig. S10C), which correlates with higher metabolic and microglial respiratory rates in female vs male brains [38]. Together, our data demonstrate no major difference in microglial response to permanent stroke in male vs female mice.

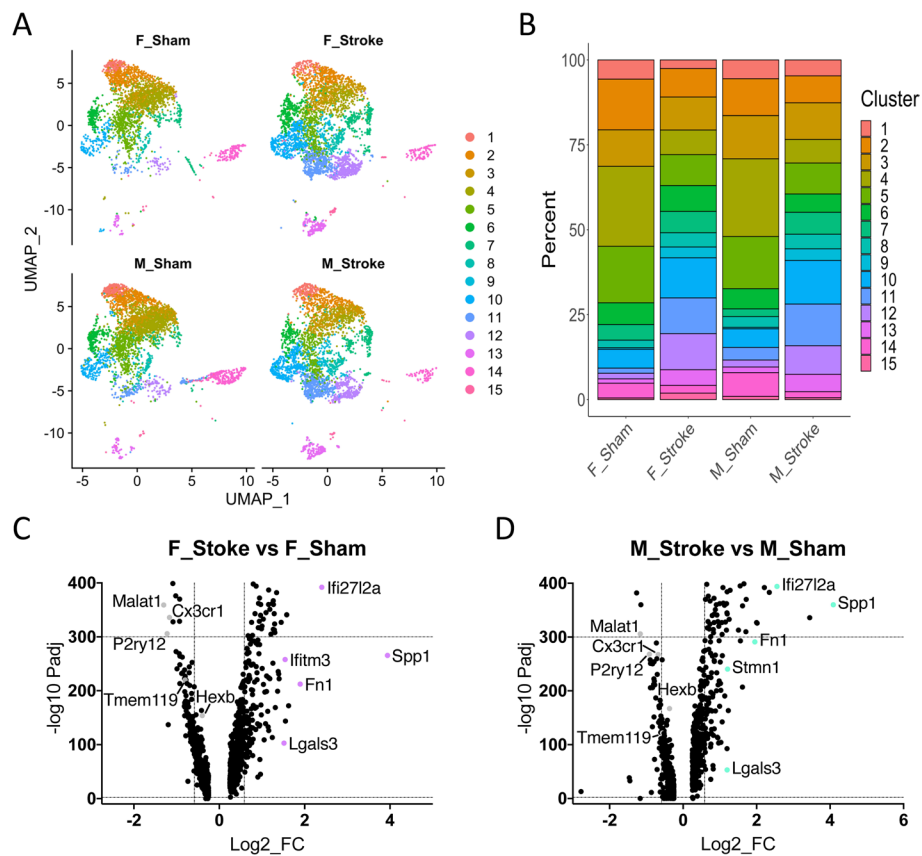


Fig. 4 Stroke-induced changes in microglia are similar between male and female mice. **A** Split view of UMAP plot of four groups: female/sham (F_Sham), female/stroke (F_Stroke), male/sham (M_Sham), and male/stroke (M_Stroke). **B** Stacked bar plots illustrating the proportions of each microglia subset in the four experimental groups. **C, D** Volcano plots showing differentially expressed genes in microglia between stroke and sham groups. The gene selection criteria are $\text{Log}_2\text{FC} > 0.25$ or < -0.25 and $p_{\text{adj}} < 0.01$. The two vertical dot lines represent fold changes of -1.5 and 1.5

Clusters 11 and 12 are DAM-like and proliferative microglia, respectively

DAM (disease-associated microglia) is one of the best-known microglial states revealed by scRNA-seq [9]. Initially identified in an Alzheimer's disease (AD) mouse, DAM was later found in other pathologic brains, such as those affected by ALS, trauma, and stroke [39]. Therefore, DAM may represent a common microglial state in response to brain damage [39]. Molecular signatures of DAM include genes such as *Spp1*, *Lpl*, *Cst7*, and *Gpnmb*. In our dataset, cluster 11 expressed several DAM genes, with *Spp1* being highly overrepresented in this cluster (Fig. 5A). However, cluster 11 did not show upregulation of some reported core DAM genes, such as *Gpnmb*. Thus, we designated cluster 11 as a DAM-like subset (Fig. 5B). We confirmed *Spp1* expression in microglia by FISH and showed that this cluster was located in the peri-infarct area (Fig. 5C). Of note, DAM-like clusters have been consistently reported in published scRNA-seq stroke studies [10–15]. Similar to our data, only a few major DAM

genes (in particular, *Spp1*) were identified in the DEGs of these reported clusters. Interestingly, many of the stroke-specific signature genes proposed in these DAM-like clusters in previous studies were also found upregulated in our cluster 11, including antioxidant genes (e.g., *Prdx1* and *Mt1/2*) [15], *Lilrb4a* [12], and *Ch25h* [14].

For cluster 12, its core signature genes (e.g., *Top2a*, *Cdk1*, *Lig1*, and *Mki67*) clearly indicate that these microglia are highly proliferative (Fig. 5D). Pathway analysis further confirmed that almost all significantly enriched processes in cluster 12 were related to cell proliferation (Additional file 1: Fig. S11A). Many cell cycle-related genes were upregulated in this cluster, and their function is involved in almost every step of the cell cycle (Additional file 6: Table S3). Our data further confirmed colocalization of the MKi67 or BrdU signal with ZsGreen, analyzed by FISH and immunofluorescence, respectively (Fig. 5E). Lastly, cell cycle score analysis indicated a marked increase of cluster 12 microglia in the G2/M phase (Fig. 5F).

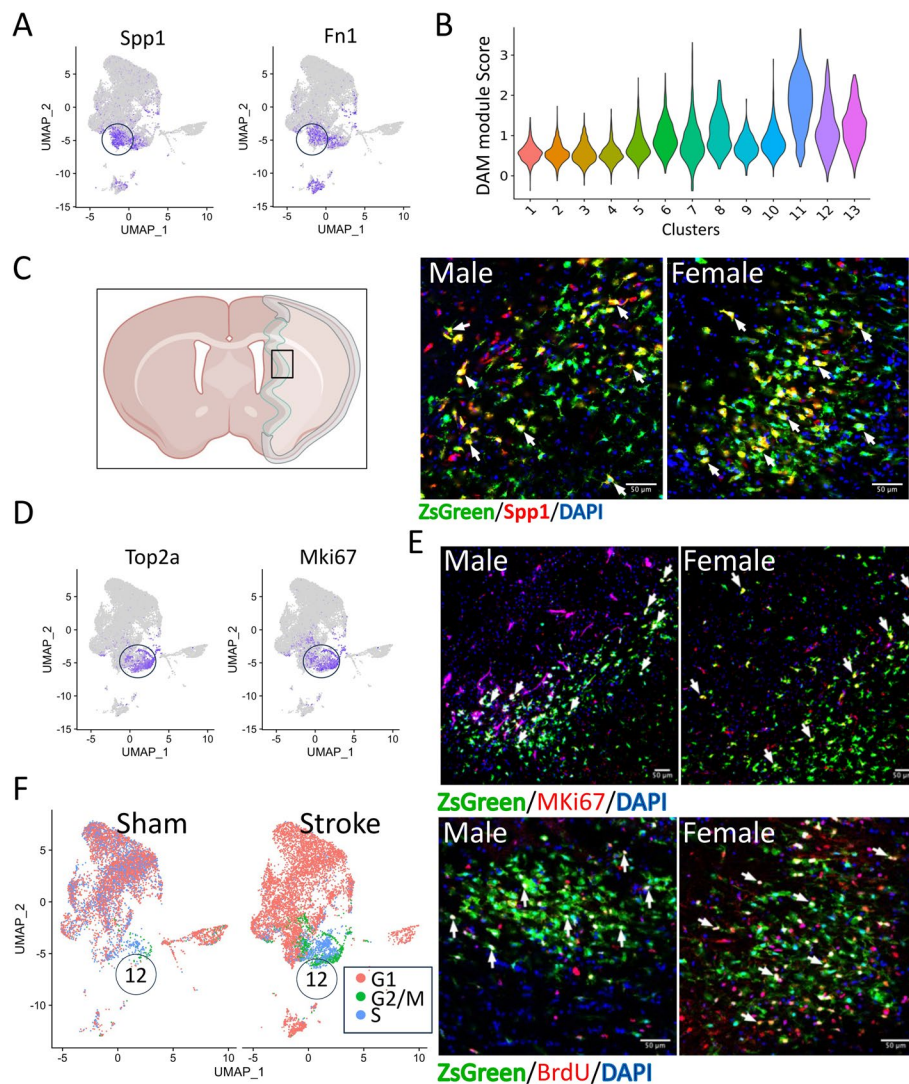


Fig. 5 Clusters 11 and 12 microglia. **A–C** Cluster 11 microglia express some signature genes of DAM. **A** UMAP plots showing two top highly expressed genes in cluster 11. **B** DAM module score analysis. **C** Representative images of *Spp1* fluorescence in situ hybridization (FISH) in peri-infarct areas on day 3 after stroke. Arrows (white) indicate ZsGreen⁺*Spp1*⁺ microglia. **D–F** Cluster 12 microglia exhibit high expression of genes related to cell proliferation. **D** Feature plots showing 2 top highly expressed genes in cluster 12. **E** Representative images of MKi67 (FISH) and BrdU (immunofluorescence) staining in peri-infarct areas on day 3 after stroke. Arrows (white) indicate ZsGreen⁺MKi67⁺ or ZsGreen⁺BrdU⁺ microglia. **F** A substantial portion of cluster 12 microglia are in the G2/M phase

Cluster 13 may constitute a unique microglial population showing macrophage-like properties

In the UMAP, cluster 13 exhibited a notable departure from the other microglial clusters (Fig. 3C). Interestingly, many of its marker genes are typically expressed in macrophages, such as *Arg1*, *Ccr2*, *S100a6*, and *Cybb* (Fig. 6A). We confirmed *Arg1* expression in some ZsGreen⁺ microglia in the peri-infarct area by FISH (Fig. 6B). As expected, most *Arg1*⁺ cells were not ZsGreen positive, representing infiltrating monocytes. It is important to note that in *Tmem119*-Ai6 mice,

once microglia were labeled with tamoxifen-induced ZsGreen, ZsGreen expression was independent of the *Tmem119* promoter activity. Thus, even if *Tmem119* is induced in cells other than microglia after stroke, these cells are still ZsGreen negative due to the absence of tamoxifen treatment. In light of this and the substantial presence of this cluster (4.6% and 5.1% of all microglia in females and males, respectively), we consider that cluster 13 represents microglia with macrophage-like properties after stroke. Of note, a previous study

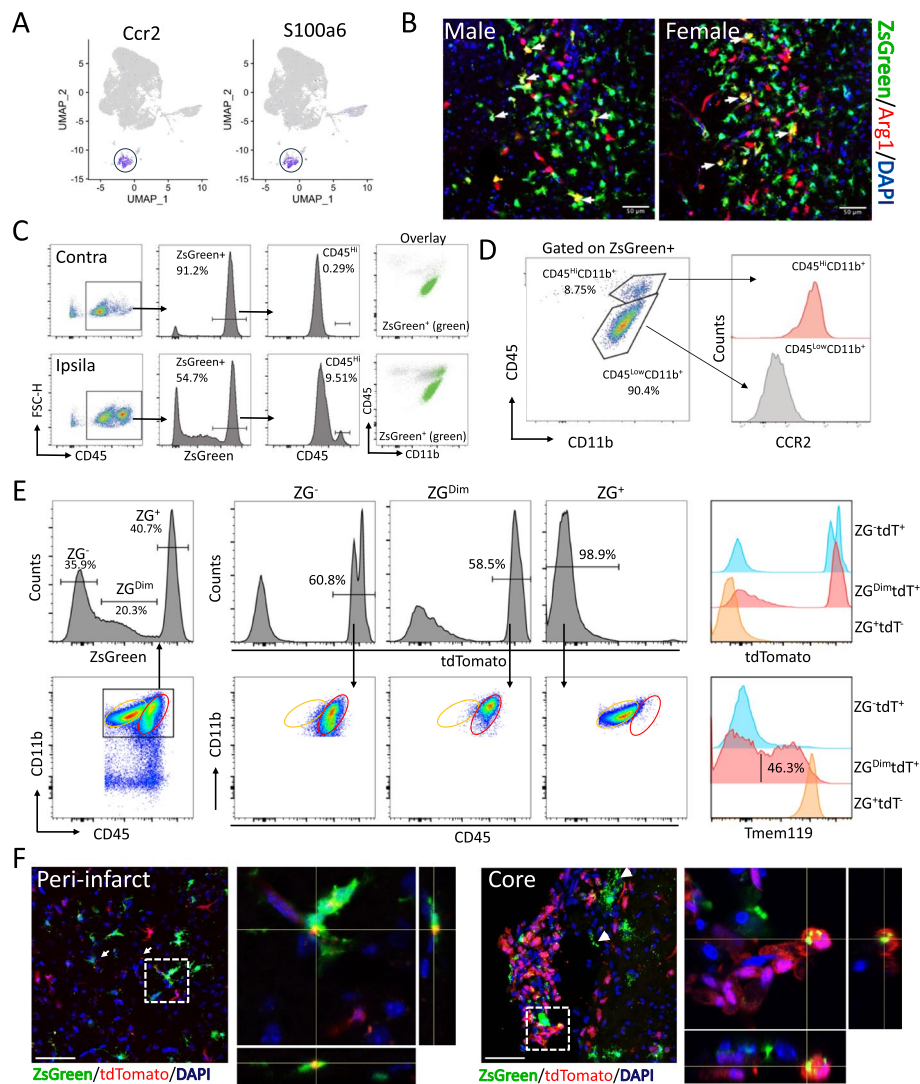


Fig. 6 Cluster 13 may represent a stroke-induced subpopulation of microglia with increased CD45 expression and macrophage properties. **A** Feature plots showing two top highly expressed genes in cluster 13. **B** Representative images of *Arg1* fluorescence in situ hybridization (FISH) in peri-infarct areas of Tmem119-Ai6 mouse brains on day 3 after permanent stroke. Arrows (white) indicate ZsGreen⁺Arg1⁺ microglia. **C, D** ZsGreen⁺ microglia in the stroke brain. Tmem119-Ai6 mice were subjected to permanent stroke. On day 3 after stroke, single-cell suspensions were prepared from contralateral (contra) and ipsilateral (ipsila) hemispheres for flow cytometric analysis. **C** CD45 expression was increased in a subpopulation of ZsGreen⁺ cells. Representative gated plots were shown for analysis of ZsGreen⁺ cells. **D** CD45^{Hi}ZsGreen⁺ cells likely correspond to cluster 13 microglia. ZsGreen⁺ cells in the CD45^{Hi}CD11b⁺ population express CCR2, a signature marker of cluster 13. **E, F** ZsGreen^{Dim}tdTomato⁺ cells in the stroke brain. Chimera mice (microglia labeled with ZsGreen and periphery immune cells labeled with tdTomato) were subjected to permanent stroke. On day 3 after stroke, flow cytometry analysis (**E**) and confocal imaging (**F**) were performed. **E** CD45⁺CD11b⁺ cells were further analyzed. ZG: ZsGreen, tdT: tdTomato. **F** Representative orthogonal views of confocal images show phagocytosis of ZsGreen⁺ microglia and tdTomato⁺ immune cells. The xy images are presented as maximal projections of z stacks. Arrows depict tdTomato fluorescent dots and arrow heads depict punctate structures with ZsGreen signal. Data are representative of at least three independent experiments

suggested that infiltrated monocytes can transform into microglia after stroke [40].

To identify this cluster by flow cytometry, we first analyzed brain immune cells from Tmem119-Ai6 mice after stroke and found that a subpopulation of ZsGreen⁺ cells in the ipsilateral brain emerged in the

gate of CD45^{Hi}CD11b⁺ (Fig. 6C). When analyzing only ZsGreen⁺ cells, we observed an obvious increase in CD45 expression in a certain population of microglia (Fig. 6C). Quantitative analysis showed that approximately 7% of ZsGreen⁺ cells were CD45^{Hi}CD11b⁺ in the ipsilateral brain after stroke (Additional file 1: Fig.

S11B). We then examine ZsGreen⁺ cells for expression of CCR2, a marker identified in cluster 13 (Fig. 6D). The data showed that CD45^{Hi}CD11b⁺ZsGreen⁺ cells expressed CCR2, suggesting that they are cluster 13 microglia. We also evaluated the phagocytic activity of CD45^{Hi}CD11b⁺ZsGreen⁺ cells using a bead uptake assay. Consistent with previous reports, CD45^{Lo}CD11b⁺ZsGreen⁺ microglia exhibited lower phagocytic activity, compared to infiltrating monocytes/macrophages. Interestingly, CD45^{Hi}CD11b⁺ZsGreen⁺ microglia demonstrated a greater capacity for phagocytosis, compared to CD45^{Lo}CD11b⁺ZsGreen⁺ microglia (Additional file 1: Fig. S11C). These data together suggest that after a stroke, a subset of microglia (cluster 13) can acquire macrophage-like properties with high CD45 expression and increased phagocytic activity.

However, we noticed that in the ZsGreen flow cytometry histograms, the ipsilateral brain had a substantial portion of cells showing dim ZsGreen signal (between negative and positive peaks), in contrast to the contralateral hemisphere (Fig. 6C). This raised the possibility that cluster 13 cells could be infiltrating monocytes that engulfed ZsGreen⁺ microglia. To address this, we again used Tmem119-Ai6 chimera mice with BMT from Vav1-Ai9 donor mice (Fig. 2A). The CD45⁺CD11b⁺ population was further gated based on ZsGreen expression levels: negative, dim, and positive (Fig. 6E). Surprisingly, all ZsGreen^{Dim} cells resided in the CD45^{Hi}CD11b⁺ gate, with 58.5% of these cells being tdTomato positive. Of note, the immune reconstitution percentage in the blood of these chimera mice was approximately 60–70%. Thus, this indicated that most of ZsGreen^{Dim} cells also exhibited markers of infiltrating immune cells. Notably, almost half of ZsGreen^{Dim}tdTomato⁺ cells (46.3%) expressed Tmem119 (Fig. 6E), though to a lesser extent than ZsGreen⁺tdTomato⁻ microglia. These data collectively indicate that ZsGreen^{Dim}tdTomato⁺ cells comprised two cell populations: ZsGreen⁺ microglia with engulfed tdTomato and infiltrating tdTomato⁺ monocytes with engulfed ZsGreen. To further support this, we examined the stroke brain slices of the chimera mice. Indeed, many ZsGreen⁺ cells, predominantly in the peri-infarct regions, had tdTomato signal, while we also observed ZsGreen signal within tdTomato⁺ cells, particularly in the infarct core (Fig. 6F). Further, in the core region, punctate structures with ZsGreen signal were evident, indicating dying microglia or microglial debris (Fig. 6F). Thus, the data suggest that on day 3 after stroke, infiltrating immune cells were responsible for clearing dead microglia in the infarct. Moreover, the presence of tdTomato fluorescent dots manifested dead

infiltrating tdTomato⁺ immune cells. Taken together, we provided evidence that cluster 13 cells are likely CD45^{Hi}CD11b⁺ZsGreen^{Dim}Tmem119^{Low} microglia, which may play a crucial role in the clearance of dead infiltrating immune cells during the acute phase of stroke.

Cluster 10 microglia exhibited activation of IFN signaling evidenced by upregulation of many IFN-related genes

Our data indicate that cluster 10 is the most abundant microglia cluster in both female (11.8%) and male (12.8%) stroke brains (Additional file 1: Fig. S10B). In cluster 10 microglia (Fig. 7), many IFN stimulated genes (ISGs; e.g., *Isg15* and *Ifit3*) and IFN regulatory genes (*Irf7*, *Stat1*, and *Stat2*) were upregulated (Fig. 7A,C). Pathway analysis identified processes related to IFN responses (Fig. 7B), which is also reflected by type I IFN response module score analysis (Fig. 7D). Analysis of *Isg15* expression in ZsGreen⁺ microglial cells by FISH indicated that they were mainly located within the peri-infarct region (Fig. 7E).

Notably, cluster 10 microglia exhibited a marked upregulation of *Stat1* (Fig. 7C), a key mediator in IFN signaling. Importantly, McDonough et al. [41] reported that after stroke, ISGs (e.g., *Irf7*, *Ifit1*, and *Ifit2*) are upregulated, likely via the STAT1 phosphorylation pathway. Thus, the STAT1 signaling pathway may play a critical role in stroke progression, making it a potential therapeutic target. To test this, we used fludarabine, a STAT1-specific inhibitor. In the first short-term stroke experiment (Fig. 8A), we mainly focused on the effect of fludarabine on infarct size. Male mice received fludarabine treatment 30 min after permanent MCA ligation, followed by two additional injections on days 1 and 2 post stroke. Both rotarod test and infarct measurement showed no significant difference between vehicle and treatment groups (Fig. 8B,C). Next, we performed a long-term functional stroke outcome study (Fig. 8D–G). As expected, mice from both groups demonstrated functional recovery over time, evident in neurologic score and pole test. Critically, compared to the vehicle group, fludarabine-treated mice showed significantly better neurologic scores 3 weeks after permanent stroke (Fig. 8E). Moreover, cognitive function after stroke, as assessed in the Y maze test, was improved with fludarabine treatment (Fig. 8G). Collectively, our data suggest that the microglial subset with upregulated *Stat1* may be detrimental for functional recovery after stroke.

Discussion

Here, we performed the first scRNA-seq analysis of microglia enriched from both male and female mouse brains after permanent stroke. Our data indicate that

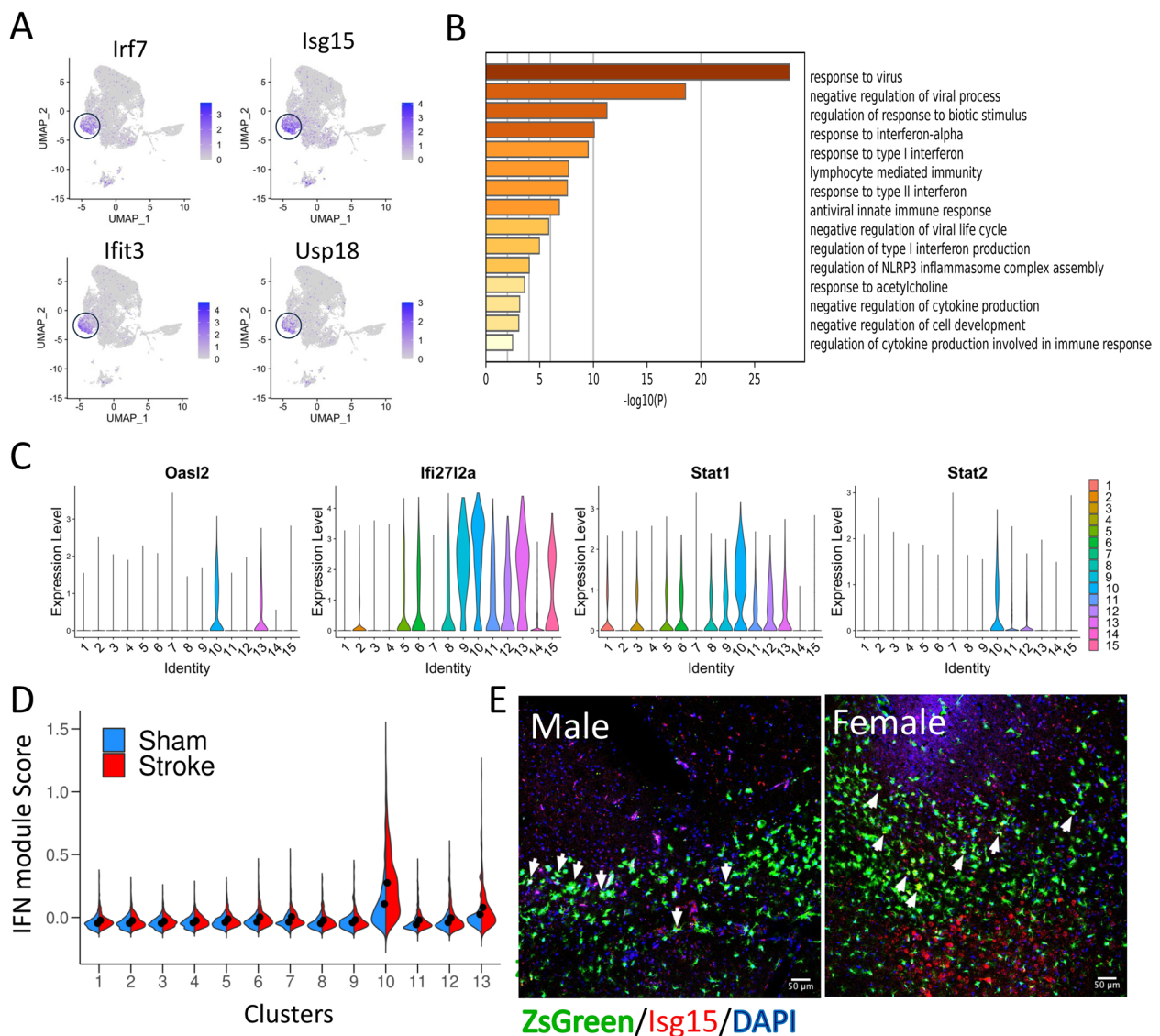


Fig. 7 Cluster 10 microglia exhibit upregulated expression of IFN-related genes. **A** Feature plots showing the 4 top highly expressed genes in cluster 10 microglia. **B** Bar plots depicting the top activated GO biological processes in cluster 10 microglia. **C** Violin plots illustrating the expression levels of IFN-related genes. **D** IFN module score analysis. **E** Representative images of *Isg15* fluorescence in situ hybridization (FISH) in peri-infarct areas of Tmem119-Ai6 mouse brains on day 3 after permanent stroke. Arrows (white) indicate ZsGreen⁺*Isg15*⁺ microglia

stroke markedly shapes the molecular landscape of microglia, resulting in diverse microglial states in the post-stroke brain. Notably, no major sex-difference in microglial response to stroke was found in our study. Based on our results, we propose that there are at least seven SAM states, represented by our clusters 7–13. Of particular importance, we provide the first evidence that cluster 13 may represent stroke-induced CD45^{Hi} microglia with macrophage-like properties and elevated phagocytic activity. Moreover, our functional outcome data suggest that inhibiting STAT1, a major regulator of IFN response that is markedly upregulated in cluster 10

microglia, is beneficial for long-term recovery after permanent ischemic stroke.

Unlike published scRNA-seq studies in stroke, the current study sequenced FACS-isolated microglia, which may allow us to achieve a higher resolution in understanding the molecular landscape of microglia. Indeed, our analysis led to the identification of at least 13 different microglial states. Even for homeostatic states, six clusters were revealed. However, it should be noted that these clusters showed largely subtle differences in transcriptional profiles between them, as evidenced by low fold changes even in the top DEG markers of each cluster

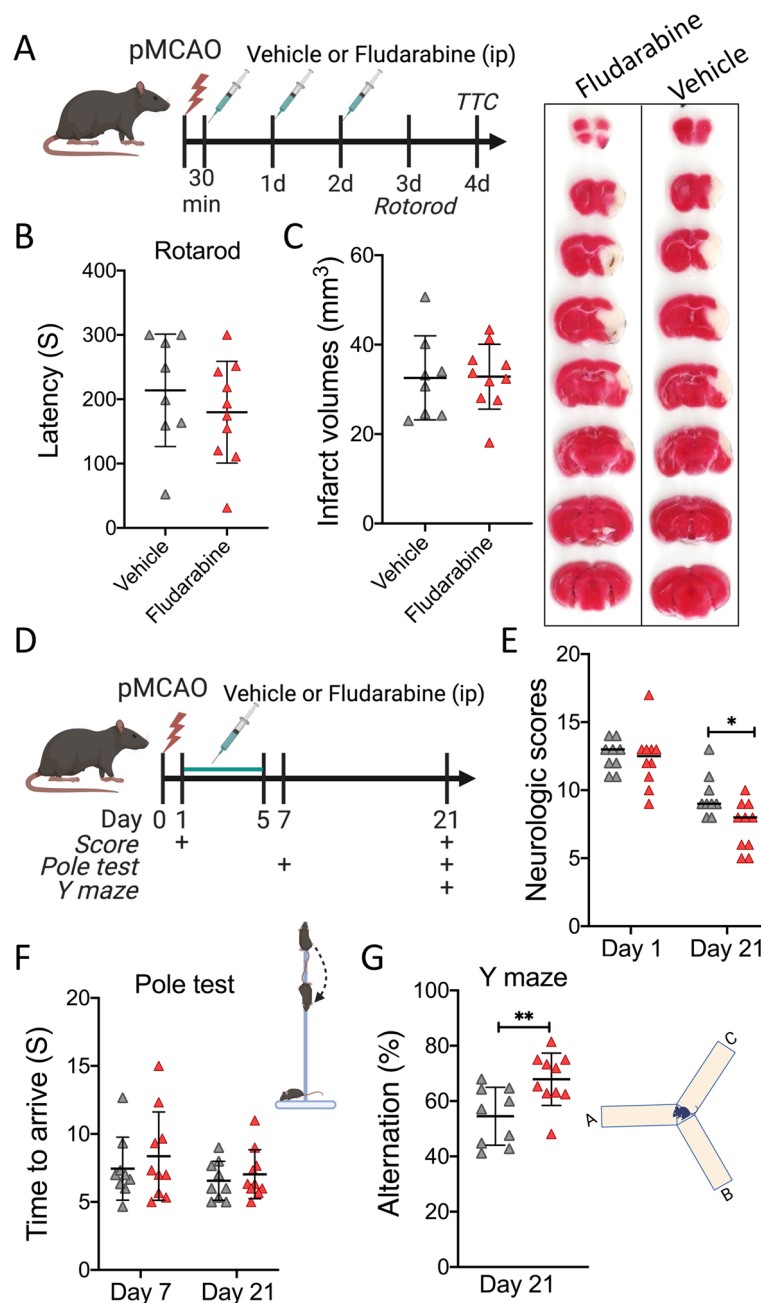


Fig. 8 Inhibition of STAT1 signaling improves long-term stroke outcome. **A–C** Short-term stroke outcome. **A** Experimental design. **B, C** Mice ($n=7$ or 10 /group) were subjected to pMCAO. Rotarod test was performed on day 3 after stroke (**B**). On post-stroke day 4, infarct volumes were measured (**C**). Representative TTC-stained brain sections are shown. **D–G** Long-term stroke outcome. **D** Experimental design. **E–G** Mice ($n=9$ – 10 /group) were subjected to pMCAO. Starting on day 1 post stroke, mice were treated with vehicle or fludarabine daily for 5 days. Behavioral tests, including neurologic scoring (**E**), pole test (**F**), and Y maze test (**G**), were performed over 21 days after stroke. Data are presented as mean \pm SD or median. *, $p < 0.05$; **, $p < 0.01$

(Additional file 6: Table S3). Among these clusters, the relatively distinct subsets are clusters 1 and 2 with upregulation of early response genes (e.g., *Jun* and *Fos*) and cluster 6 with high *ApoE* expression. These homeostatic microglial subsets, even with small transcriptional

differences, may reflect diverse, dynamic, and multidimensional functions of microglia in the physiologic state [39].

We identified a total of 7 potential SAM states and performed further analyses on 4 clusters (clusters 10–13).

So far, several scRNA-seq studies have attempted to name certain clusters as SAM [12, 14, 15]. For example, Kim et al. performed scRNA-seq analysis on brain cells collected at 24 h and 48 h after 60-min transient MCAO [15]. Only two microglial clusters were identified, with one cluster annotated as SAM. This SAM cluster expresses some DAM signature genes as well as antioxidant genes (e.g., *Prdx1* and *Mt1/2*). They further provided evidence that deletion of *Prdx1* is detrimental to stroke, suggesting a protective role of this SAM subset. Recently, another scRNA-seq study proposed three SAM clusters, which were named as MKI67⁺, CH25H⁺, and OASL⁺ [14]. Among these clusters, MKI67⁺ microglia express many cell cycle-related genes (e.g., *Top2a*), CH25H⁺ microglia show expression of some DAM genes (e.g., *Spp1* and *Fn1*), and OASL⁺ microglia exhibit robust upregulation of interferon response genes (e.g., *Irf7* and *Ifi2712a*). The authors also demonstrated that *Ch25h* knockout mice have worse stroke outcome, again suggesting that DAM-like microglia could be beneficial in stroke. Beuker et al. performed an scRNA-seq analysis of CD45⁺ cells from the brain after transient MCAO [12]. Notably, they proposed one macrophage-like cluster as stroke-associated myeloid cells (SAMC). Cells in this cluster express genes found in developing and DAM microglia, such as *Spp1*, *Fth1*, *Lgals3*, *Lyz2*, *ApoE*, *Gpnmb*, and *Fabp5*. Based on these signature genes, it appears that SAMC is a combination of our clusters 11 and 13. Indeed, using BMT chimeras, they showed that SAMC derived mainly from microglia. Collectively, our study identified not only all the published SAM clusters with a higher resolution, but also new ones. For example, our analysis revealed a unique cluster of the microglia-derived macrophage-like cells (cluster 13), a subset that was not identified previously due to technical limitations.

This is the first scRNA-seq study designed to determine sex difference in microglial response to permanent stroke. In the literature, sex difference in microglia in vivo functions has not been well established, as most studies were performed in cultured cells. Some animal studies reported sex differences in regional cell density, cell size, and morphology of microglia in the brain, but similar basal phagocytosis activity of microglia between sexes [42, 43]. Sex dimorphism in microglial activation after stroke is also not well studied [21]; however, it has been thought that microglial activation may be sex-dependent and thus contribute to brain damage differentially after stroke. This notion is supported primarily by a finding that microglia from female mice transplanted into male mouse brains provide protective effects after stroke [44]. Although their data showed that transplanted female microglia comprise only ~20% of the total microglia in male brains, the extent of the protective effects in

males was similar to females. Also, they found no sex difference in stroke outcome if male microglia were transplanted into female brains. Thus, this important finding needs to be further confirmed, and more studies are required to clarify the role of microglia in sex differences in the post-stroke immune response. Using bulk RNA-seq analysis, studies indeed reported sex-specific differences in the microglial transcriptome in the healthy brain [43, 44]. However, our scRNA-seq analysis of microglia detected only minor sex differences within either sham or stroke groups. The discrepancy may result from the limitations of different techniques, as bulk RNA-seq is normally used to identify changes in gene expression between conditions, while scRNA-seq is better suited to reveal cell heterogeneity (e.g., subpopulations and dynamic states). Nevertheless, another scRNA-seq study also failed to reveal any major differences in microglial diversity between intact male and female brains [45].

The use of *Tmem119-Ai6* mice provided a unique advantage for examining microglia in a highly specific manner. This led to the discovery of cluster 13, which may represent CD45^{Hi} microglia, a population that has been largely unexplored in stroke research. The oversight is partly due to the current CD45-based flow cytometry approach in studying microglia. One of the distinctive features of microglia is low CD45 expression, compared to peripheral immune cells. Therefore, in the stroke field, most studies apply a standard gating strategy in which CD45^{Hi}CD11b⁺ cells are regarded as infiltrating myeloid cells, while the CD45^{Lo}CD11b⁺ population is considered microglia. Our data demonstrated that indeed, in the healthy brain, almost all microglia labeled with ZsGreen belong to the CD45^{Lo}CD11b⁺ population. However, after stroke, CD45 expression in some microglia may be increased, placing a subset of microglia in the CD45^{Hi}CD11b⁺ gate. Consistent with this notion, previous studies have suggested the presence of CD45^{Hi}CD11b⁺ microglia in the stroke brain [12, 46, 47]. Using the microglia-specific markers *Tmem119* and *P2RY12* in flow cytometry analysis, one study reported that around 22% of CD45^{Hi}CD11b⁺ cells are likely microglia [46]. As mentioned above, one scRNA-seq study identified a stroke-specific myeloid cell cluster (SAMC) expressing macrophage markers with a high level of CD45 [12]. The authors found that this cluster is comprised of microglia [12]. Moreover, transcriptomic studies also found that *Ccr2* expression is induced in microglia after stroke [47, 48]. In line with these studies, our flow cytometry data revealed that in the stroke brain, a subpopulation of microglia exhibited moderate ZsGreen signal with low expression of *Tmem119* and increased expression of CD45 and *CCR2* (Fig. 6). Importantly, our data further showed that these cells exhibited

high phagocytic activity and may actively engulf cellular debris from dead infiltrating immune cells.

Microglial subsets with high expression of ISGs have been identified in the stroke brain by previous scRNA-seq analysis [10, 13, 14]. This aligns with a number of studies indicating that the IFN pathways, in particular type I IFN (IFN-I) response, are activated after stroke. For example, a large-scale RNA-seq analysis proposed that IFN-I signaling activation is a hallmark of the differential response of aged vs young animals to stroke [49], with ISG expression peaking earlier in young mice and sustaining longer in aged mice. Further regulatory network analysis suggests that STAT1 is involved in upregulation of ISGs. In our scRNA-seq analysis, cluster 10 showed overrepresentation of many IFN-related genes, including *Irf7* and *Stat1*. Another recent scRNA-seq study also identified a similar cluster, referred to as OASL⁺microglia, in the brain after transient stroke and suggested that IRF7 is a major regulator of stroke-induced ISGs in microglia [14]. Interestingly, in vitro data indicate that IRF7 and STAT1 together drive transition of microglial states [50]. Thus, future studies may focus on these two signaling regulators to better understand how IFN response in microglia is regulated in the stroke brain. Certainly, it is also critical to clarify the role of this microglial subset in stroke outcome because our data indicate that cluster 10 accounts for a dominant microglia state in the stroke brain (Additional file 1: Fig. S8A). As an initial attempt, we used fludarabine to inhibit STAT1 signaling and examined its effects on stroke outcome. Of note, in our long-term outcome study, we used a permanent ischemic stroke model, the first dose of fludarabine was given 24 h after stroke, and neurologic deficit was evaluated 3 weeks after stroke. This experimental design is of high clinical relevance because most ischemic stroke patients cannot reach the hospital in time for acute reperfusion therapy, and long-term functional recovery defines the quality of life in stroke patients. Interestingly, we found that fludarabine treatment did not reduce infarct volumes in the short-term stroke experiment, but improved functional outcome 3 weeks after stroke. Agreeing with our data, a recent study demonstrated upregulation of *Stat1* in microglia after transient stroke, and deletion of *Stat1* in both microglia and monocytes results in significant improvement in long-term, but not acute (24 h after stroke), stroke outcome [51]. Together, these findings provide strong evidence that (1) cluster 10 microglia are present in the stroke brain; (2) these microglia may exert detrimental effects on stroke recovery; and (3) STAT1 could be a therapeutic target to improve long-term stroke outcome.

Several limitations of this study are noted. First, for clusters 10–13, we only validated one prominent

signature gene for each cluster using FISH. To precisely define each cluster, a combination of marker genes is required. Second, it remains unknown how cluster 13 microglia affect stroke outcome. To clarify this, it would be necessary to identify major regulatory pathways driving the transition of this cluster in future studies. Third, the massive presence of microglia in the infarct core on day 7 after stroke is striking and warrants further research. Lastly, although our study demonstrated for the first time that post-stroke fludarabine treatment improved long-term functional outcome after permanent stroke, this treatment is not microglia-specific. However, multiple lines of evidence suggest that activation of STAT1 signaling primarily occurs in microglia in the stroke brain [41, 51]. Recently, one study has used Cx3cr1^{CreER} mice in a stroke study to conditionally delete *Stat1* in both microglia and macrophages [51]. Nonetheless, microglia-specific *Stat1* knockout mice are still needed to clarify the role of the IFN microglia cluster in stroke.

Conclusions

Our findings revealed the diverse responses of microglia to ischemic stroke and underscored the importance of understanding microglial heterogeneity in stroke pathology. Future studies should be designed to elucidate the functional significance of the SAM subsets identified here and their potential implications for stroke therapy. This line of research may eventually inform the development of novel and effective immunomodulatory stroke therapies by targeting specific microglial populations.

Supplementary Information

The online version contains supplementary material available at <https://doi.org/10.1186/s13073-024-01368-7>.

Additional file 1: Table S1. List of antibodies. Table S2. Gene list for module score analysis. Figure S1. Iba1⁺ cells in the different regions of the stroke brain. Figure S2. Characterization of Tmem119-Ai6 mice in stroke. Figure S3. Flow cytometry analysis of tdTomato⁺ cells in the blood of the chimera mice. Figure S4. Infiltrating immune cells in the stroke brain. Figure S5. Phagocytic capacity of microglia is markedly increased on day 7 after stroke. Figure S6. Time-course of the spatial distribution of infiltrating tdTomato⁺ immune cells in the stroke brains. Figure S7. Stroke-induced changes in microglia revealed by scRNA-seq analysis. Figure S8. Stroke-induced microglia states. Figure S9. Comparison of stroke outcome between male and female mice. Figure S10. Microglia respond to stroke similarly between male and female mice. Figure S11. Clusters 12 and 13.

Additional file 2: Movie S1. A video clip of coronal sections of the brain on day 1 after stroke. A chimeric Tmem119-Ai6 mouse was generated by transplantation of bone marrow cells from a Vav1-Ai9 mouse. The chimeric mouse was subjected to permanent middle cerebral artery occlusion, and the brain was collected on day 1 after stroke. The cleared brain was then stained with NeuN. The brain was imaged with a light-sheet microscope. In this video, neurons are labelled in blue, microglia in green, and infiltrating immune cells in red.

Additional file 3: Movie S2. A video clip of coronal sections of the brain on day 3 after stroke. A chimeric Tmem119-Ai6 mouse was generated by transplantation of bone marrow cells from a Vav1-Ai9 mouse. The chimeric mouse was subjected to permanent middle cerebral artery occlusion, and the brain was collected on day 3 after stroke. The cleared brain was then stained with NeuN. The brain was imaged with a light-sheet microscope. In this video, neurons are labelled in blue, microglia in green, and infiltrating immune cells in red.

Additional file 4: Movie S3. Visualization of 3D reconstruction of the brain on day 3 after stroke showing distribution of microglia. A chimeric Tmem119-Ai6 mouse was generated by transplantation of bone marrow cells from a Vav1-Ai9 mouse. The chimeric mouse was subjected to permanent middle cerebral artery occlusion, and the brain was collected on day 3 after stroke. The cleared brain was then stained with NeuN. The brain was imaged with a light-sheet microscope. In this video, neurons are labelled in blue and microglia in green.

Additional file 5: Movie S4. Visualization of 3D reconstruction of the brain on day 7 after stroke showing distribution of infiltrating immune cells. A chimeric C57Bl/6 mouse was generated by transplantation of bone marrow cells from a Vav1-Ai9 mouse. The chimeric mouse was subjected to permanent middle cerebral artery occlusion, and the brain was collected on day 7 after stroke. The cleared brain was then stained with NeuN. The brain was imaged with a light-sheet microscope. In this video, neurons are labelled in blue and infiltrating immune cells in red.

Additional file 6: Table S3. This file has 15 worksheet tabs. Each tab contains the top 50 genes enriched in the corresponding cluster.

Additional file 7: Table S4. The list of differentially expressed genes between stroke and sham. The analysis was performed on aggregated data. This file has 2 worksheet tabs. The first tab contains the genes used to generate the volcano plot, and the second tab contains the genes used for pathway analysis.

Additional file 8: Table S5. The lists of differentially expressed genes of different comparisons. This file has 4 worksheet tabs that contain DEGs from the following comparisons: F_stroke vs F_sham, M_stroke vs M_sham, F_sham vs M_sham, and F_stroke vs M_stroke. The selection criteria are: $p_{adj} < 0.01$ and fold-change ≥ 1.5 or ≤ -1.5 .

Acknowledgements

We thank Pei Miao for her excellent technical support, and Kathy Gage for her excellent editorial contribution. Scheme figures were created with BioRender.com

Authors' contributions

Conceptualization: ÁÁ and WY. Methodology: ÁÁ, RZ, XY, LD, FX, JZ, VJ, JT, XPZ, HS, and WY. Supervision: ÁÁ, HS, and WY. Writing: ÁÁ and WY. All authors read and approved the final manuscript.

Funding

This study was supported by funds from the Department of Anesthesiology (Duke University Medical Center) and NIH grants NS099590, HL157354, and NS127163.

Availability of data and materials

The single-cell RNA sequencing dataset has been deposited in NCBI Gene Expression Omnibus (GEO) database repository with the accession number GSE267240 (<https://www.ncbi.nlm.nih.gov/geo/query/acc.cgi?acc=gse267240>).³⁰ Other data are available from the corresponding author on reasonable request. Please allow 3 weeks for responses.

Declarations

Ethics approval and consent to participate

All animal procedures were approved by the Duke University Medical Center Animal Care and Use Committee and were conducted in accordance with the United States Public Health Service's Policy on Humane Care and Use of Laboratory Animals.

Consent for publication

Not applicable.

Competing interests

The authors declare that they have no competing interests.

Author details

¹Multidisciplinary Brain Protection Program, Department of Anesthesiology, Duke University Medical Center, 303 Research Drive, Box 3094, Durham, NC 27710, USA. ²Duke Molecular Physiology Institute, Duke University School of Medicine, Durham, NC, USA. ³Department of Biostatistics and Bioinformatics, Duke University School of Medicine, Durham, NC, USA. ⁴Departments of Pediatrics and Integrative Immunobiology, Duke University Medical Center, Durham, NC, USA. ⁵Department of Neurology, Duke University Medical Center, Durham, NC, USA.

Received: 7 January 2024 Accepted: 23 July 2024

Published online: 02 August 2024

References

- Tsao CW, Aday AW, Almarzooq ZI, Anderson CAM, Arora P, Avery CL, Baker-Smith CM, Beaton AZ, Boehme AK, Buxton AE, et al. Heart disease and stroke statistics-2023 update: a report from the American Heart Association. *Circulation*. 2023;147:e93–621. <https://doi.org/10.1161/CIR.0000000000001123>.
- Iadecola C, Anrather J. The immunology of stroke: from mechanisms to translation. *Nat Med*. 2011;17:796–808. <https://doi.org/10.1038/nm.2399>.
- Iadecola C, Buckwalter MS, Anrather J. Immune responses to stroke: mechanisms, modulation, and therapeutic potential. *J Clin Invest*. 2020;130:2777–88. <https://doi.org/10.1172/JCI135530>.
- Zhang SR, Phan TG, Sobey CG. Targeting the immune system for ischemic stroke. *Trends Pharmacol Sci*. 2021;42:96–105. <https://doi.org/10.1016/j.tips.2020.11.010>.
- Xu S, Lu J, Shao A, Zhang JH, Zhang J. Glial cells: role of the immune response in ischemic stroke. *Front Immunol*. 2020;11:294. <https://doi.org/10.3389/fimmu.2020.00294>.
- Dong R, Huang R, Wang J, Liu H, Xu Z. Effects of microglial activation and polarization on brain injury after stroke. *Front Neurol*. 2021;12:620948. <https://doi.org/10.3389/fneur.2021.620948>.
- Wang Y, Leak RK, Cao G. Microglia-mediated neuroinflammation and neuroplasticity after stroke. *Front Cell Neurosci*. 2022;16:980722. <https://doi.org/10.3389/fncel.2022.980722>.
- Jin WN, Shi SX, Li Z, Li M, Wood K, Gonzales RJ, Liu Q. Depletion of microglia exacerbates postischemic inflammation and brain injury. *J Cereb Blood Flow Metab*. 2017;37:2224–36. <https://doi.org/10.1177/0271678X17694185>.
- Masuda T, Sankowski R, Staszewski O, Prinz M. Microglia heterogeneity in the single-cell era. *Cell Rep*. 2020;30:1271–81. <https://doi.org/10.1016/j.celrep.2020.01.010>.
- Zheng K, Lin L, Jiang W, Chen L, Zhang X, Zhang Q, Ren Y, Hao J. Single-cell RNA-seq reveals the transcriptional landscape in ischemic stroke. *J Cereb Blood Flow Metab*. 2021;27:1678X211026770. <https://doi.org/10.1177/0271678X211026770>.
- Shi L, Sun Z, Su W, Xu F, Xie D, Zhang Q, Dai X, Iyer K, Hitchens TK, Foley LM, et al. Treg cell-derived osteopontin promotes microglia-mediated white matter repair after ischemic stroke. *Immunity*. 2021;54(1527–1542):e1528. <https://doi.org/10.1016/j.immuni.2021.04.022>.
- Beuker C, Schafflick D, Strecker JK, Heming M, Li X, Wolbert J, Schmidt-Pogoda A, Thomas C, Kuhlmann T, Aranda-Pardos I, et al. Stroke induces disease-specific myeloid cells in the brain parenchyma and pia. *Nat Commun*. 2022;13:945. <https://doi.org/10.1038/s41467-022-28593-1>.
- Li X, Lyu J, Li R, Jain V, Shen Y, Del Águila A, Hoffmann U, Sheng H, Yang W. Single-cell transcriptomic analysis of the immune cell landscape in the aged mouse brain after ischemic stroke. *J Neuroinflammation*. 2022;19:83. <https://doi.org/10.1186/s12974-022-02447-5>.
- Zhang Y, Guo Y, Li R, Huang T, Li Y, Xie W, Chen C, Chen W, Wan J, Yu W, et al. Novel CH25H(+) and OASL(+) microglia subclusters play distinct roles in cerebral ischemic stroke. *J Neuroinflammation*. 2023;20:115. <https://doi.org/10.1186/s12974-023-02799-6>.

15. Kim S, Lee W, Jo H, Sonn SK, Jeong SJ, Seo S, Suh J, Jin J, Kweon HY, Kim TK, et al. The antioxidant enzyme Peroxiredoxin-1 controls stroke-associated microglia against acute ischemic stroke. *Redox Biol.* 2022;54:102347. <https://doi.org/10.1016/j.redox.2022.102347>.
16. Garcia-Bonilla L, Shahanoor Z, Sciortino R, Nazarzoda O, Racchumi G, Iadecola C, Anrather J. Analysis of brain and blood single-cell transcriptomics in acute and subacute phases after experimental stroke. *Nat Immunol.* 2024;25:357–70. <https://doi.org/10.1038/s41590-023-01711-x>.
17. Han B, Zhou S, Zhang Y, Chen S, Xi W, Liu C, Zhou X, Yuan M, Yu X, Li L, et al. Integrating spatial and single-cell transcriptomics to characterize the molecular and cellular architecture of the ischemic mouse brain. *Sci Transl Med.* 2024;16:eadg1323. <https://doi.org/10.1126/scitranslmed.adg1323>.
18. Kaiser T, Feng G. Tmem119-EGFP and Tmem119-CreERT2 Transgenic mice for labeling and manipulating microglia. *eNeuro.* 2019;6. <https://doi.org/10.1523/ENEURO.0448-18.2019>.
19. McBride DW, Zhang JH. Precision Stroke Animal Models: the Permanent MCAO Model Should Be the Primary Model. *Not Transient MCAO Transl Stroke Res.* 2017. <https://doi.org/10.1007/s12975-017-0554-2>.
20. Jiang M, Yu S, Yu Z, Sheng HX, Li Y, Liu S, Warner DS, Paschen W, Yang W. XBP1 (X-box-binding protein-1)-dependent O-GlcNAcylation is neuroprotective in ischemic stroke in young mice and its impairment in aged mice is rescued by thiamet-G. *Stroke.* 2017;48:1646–54.
21. Ugidos IF, Pistono C, Korhonen P, Gomez-Budia M, Sitnikova V, Klecki P, Stanova I, Jolkonen J, Malm T. Sex differences in poststroke inflammation: a focus on microglia across the lifespan. *Stroke.* 2022;53:1500–9. <https://doi.org/10.1161/STROKEAHA.122.039138>.
22. Banerjee A, McCullough LD. Sex-specific immune responses in stroke. *Stroke.* 2022;53:1449–59. <https://doi.org/10.1161/STROKEAHA.122.036945>.
23. Sheng H, Dang L, Li X, Yang Z, Yang W. A modified transcranial middle cerebral artery occlusion model to study stroke outcomes in aged mice. *J Vis Exp.* 2023. <https://doi.org/10.3791/65345>.
24. Li X, Li R, Lu L, Dhar A, Sheng H, Yang W. Beneficial effects of neuronal ATF6 activation in permanent ischemic stroke. *Front Cell Neurosci.* 2022;16:1016391. <https://doi.org/10.3389/fncel.2022.1016391>.
25. Wang Z, Li X, Spasojevic I, Lu L, Shen Y, Qu X, Hoffmann U, Warner DS, Paschen W, Sheng H, et al. Increasing O-GlcNAcylation is neuroprotective in young and aged brains after ischemic stroke. *Exp Neurol.* 2021;339:113646. <https://doi.org/10.1016/j.expneurol.2021.113646>.
26. Zhao Y, Ma C, Chen C, Li S, Wang Y, Yang T, Stetler RA, Bennett MVL, Dixon CE, Chen J, et al. STAT1 contributes to microglial/macrophage inflammation and neurological dysfunction in a mouse model of traumatic brain injury. *J Neurosci.* 2022;42:7466–81. <https://doi.org/10.1523/JNEUROSCI.0682-22.2022>.
27. Zhao Q, Shen Y, Li R, Wu J, Lyu J, Jiang M, Lu L, Zhu M, Wang W, Wang Z, et al. Cardiac arrest and resuscitation activates the hypothalamic-pituitary-adrenal axis and results in severe immunosuppression. *J Cereb Blood Flow Metab.* 2021;41:1091–102. <https://doi.org/10.1177/0271678X20948612>.
28. McGill CJ, Lu RJ, Benayoun BA. Protocol for analysis of mouse neutrophil NETosis by flow cytometry. *STAR Protoc.* 2021;2:100948. <https://doi.org/10.1016/j.xpro.2021.100948>.
29. Park YG, Sohn CH, Chen R, McCue M, Yun DH, Drummond GT, Ku T, Evans NB, Oak HC, Trieu W, et al. Protection of tissue physicochemical properties using polyfunctional crosslinkers. *Nat Biotechnol.* 2018. <https://doi.org/10.1038/nbt.4281>.
30. del Águila A, Jain V, Yang W. Microglial heterogeneity in the ischemic stroke mouse brain of both sexes - GSE267240. *NCBI Gene Expression Omnibus Datasets.* 2024. <https://www.ncbi.nlm.nih.gov/geo/query/acc.cgi?acc=gse267240>.
31. McGinnis CS, Murrow LM, Gartner ZJ. DoubletFinder: doublet detection in single-cell RNA sequencing data using artificial nearest neighbors. *Cell Syst.* 2019;8:329–+. <https://doi.org/10.1016/j.cels.2019.03.003>.
32. Otxoa-de-Amezaga A, Miro-Mur F, Pedragosa J, Gallizioli M, Justicia C, Gaja-Capdevila N, Ruiz-Jaen F, Salas-Perdomo A, Bosch A, Calvo M, et al. Microglial cell loss after ischemic stroke favors brain neutrophil accumulation. *Acta Neuropathol.* 2019;137:321–41. <https://doi.org/10.1007/s00401-018-1954-4>.
33. Lan Y, Zhang X, Liu S, Guo C, Jin Y, Li H, Wang L, Zhao J, Hao Y, Li Z, et al. Fate mapping of Spp1 expression reveals age-dependent plasticity of disease-associated microglia-like cells after brain injury. *Immunity.* 2024;57(349–363):e349. <https://doi.org/10.1016/j.immuni.2024.01.008>.
34. Young KF, Gardner R, Sariana V, Whitman SA, Bartlett MJ, Falk T, Morrison HW. Can quantifying morphology and TMEM119 expression distinguish between microglia and infiltrating macrophages after ischemic stroke and reperfusion in male and female mice? *J Neuroinflamm.* 2021;18. <https://doi.org/10.1186/s12974-021-02105-2>.
35. Bjornholm KD, Del Gaudio F, Li H, Li W, Vazquez-Liebanas E, Mae MA, Lendahl U, Betsholtz C, Nilsson P, Karlstrom H, et al. A robust and efficient microvascular isolation method for multimodal characterization of the mouse brain vasculature. *Cell Rep Methods.* 2023;3:100431. <https://doi.org/10.1016/j.crmeth.2023.100431>.
36. Ruan C, Elyaman W. A new understanding of TMEM119 as a marker of microglia. *Front Cell Neurosci.* 2022;16:902372. <https://doi.org/10.3389/fncel.2022.902372>.
37. Brait VH, Jackman KA, Waldock AK, Selemidis S, Diep H, Mast AE, Guida E, Broughton BR, Drummond GR, Sobey CG. Mechanisms contributing to cerebral infarct size after stroke: gender, reperfusion, T lymphocytes, and Nox2-derived superoxide. *J Cereb Blood Flow Metab.* 2010;30:1306–17. <https://doi.org/10.1038/jcbfm.2010.14>.
38. Bordt EA, Ceasrine AM, Bilbo SD. Microglia and sexual differentiation of the developing brain: A focus on ontogeny and intrinsic factors. *Glia.* 2020;68:1085–99. <https://doi.org/10.1002/glia.23753>.
39. Paolicelli RC, Sierra A, Stevens B, Tremblay ME, Aguzzi A, Ajami B, Amit I, Audinat E, Bechmann I, Bennett M, et al. Microglia states and nomenclature: a field at its crossroads. *Neuron.* 2022;110:3458–83. <https://doi.org/10.1016/j.neuron.2022.10.020>.
40. Chen HR, Sun YY, Chen CW, Kuo YM, Kuan IS, Tiger Li ZR, Short-Miller JC, Smucker MR, Kuan CY. Fate mapping via CCR2-CreER mice reveals monocyte-to-microglia transition in development and neonatal stroke. *Sci Adv.* 2020;6:eabb2119. <https://doi.org/10.1126/sciadv.abb2119>.
41. McDonough A, Lee RV, Noor S, Lee C, Le T, Iorga M, Phillips JLH, Murphy S, Moller T, Weinstein JR. Ischemia/reperfusion induces interferon-stimulated gene expression in microglia. *J Neurosci.* 2017;37:8292–308. <https://doi.org/10.1523/JNEUROSCI.0725-17.2017>.
42. Han J, Fan Y, Zhou K, Blomgren K, Harris RA. Uncovering sex differences of rodent microglia. *J Neuroinflammation.* 2021;18:74. <https://doi.org/10.1186/s12974-021-02124-z>.
43. Guneykaya D, Ivanov A, Hernandez DP, Haage V, Wojtas B, Meyer N, Maricos M, Jordan P, Buonfiglioli A, Gielniewski B, et al. Transcriptional and translational differences of microglia from male and female brains. *Cell Rep.* 2018;24(2773–2783):e2776. <https://doi.org/10.1016/j.celrep.2018.08.001>.
44. Villa A, Gelosa P, Castiglioni L, Cimino M, Rizzi N, Pepe G, Lolli F, Marcello E, Sironi L, Vegeto E, et al. Sex-specific features of microglia from adult mice. *Cell Rep.* 2018;23:3501–11. <https://doi.org/10.1016/j.celrep.2018.05.048>.
45. Hammond TR, Dufort C, Dissing-Olesen L, Giera S, Young A, Wysoker A, Walker AJ, Gergits F, Segel M, Nemes J, et al. Single-cell RNA sequencing of microglia throughout the mouse lifespan and in the injured brain reveals complex cell-state changes. *Immunity.* 2019;50(253–271):e256. <https://doi.org/10.1016/j.immuni.2018.11.004>.
46. Honarpisheh P, Lee J, Banerjee A, Blasco-Conesa MP, Honarpisheh P, d'Aigle J, Mamun AA, Ritzel RM, Chauhan A, Ganesh BP, et al. Potential caveats of putative microglia-specific markers for assessment of age-related cerebrovascular neuroinflammation. *J Neuroinflammation.* 2020;17:366. <https://doi.org/10.1186/s12974-020-02019-5>.
47. Shi L, Rocha M, Zhang W, Jiang M, Li S, Ye Q, Hassan SH, Liu L, Adair MN, Xu J, et al. Genome-wide transcriptomic analysis of microglia reveals impaired responses in aged mice after cerebral ischemia. *J Cereb Blood Flow Metab.* 2020;40:549–66. <https://doi.org/10.1177/0271678X20925655>.
48. Jiang L, Mu H, Xu F, Xie D, Su W, Xu J, Sun Z, Liu S, Luo J, Shi Y, et al. Transcriptomic and functional studies reveal undermined chemotactic and angiostimulatory properties of aged microglia during stroke recovery. *J Cereb Blood Flow Metab.* 2020;40:581–97. <https://doi.org/10.1177/0271678X20902542>.
49. Androvic P, Kirdajova D, Tureckova J, Zucha D, Rohlova E, Abaffy P, Kriska J, Valny M, Anderova M, Kubista M, et al. Decoding the transcriptional response to ischemic stroke in young and aged mouse brain. *Cell Rep.* 2020;31:107777. <https://doi.org/10.1016/j.celrep.2020.107777>.

50. Tanaka T, Murakami K, Bando Y, Yoshida S. Interferon regulatory factor 7 participates in the M1-like microglial polarization switch. *Glia*. 2015;63:595–610. <https://doi.org/10.1002/glia.22770>.
51. Han W, Pu H, Li S, Liu Y, Zhao Y, Xu M, Chen C, Wu Y, Yang T, Ye Q, et al. Targeted ablation of signal transducer and activator of transduction 1 alleviates inflammation by microglia/macrophages and promotes long-term recovery after ischemic stroke. *J Neuroinflammation*. 2023;20:178. <https://doi.org/10.1186/s12974-023-02860-4>.

Publisher's Note

Springer Nature remains neutral with regard to jurisdictional claims in published maps and institutional affiliations.